CLEEN
Cluster for Energy and Environment

Research Report D413
Helsinki 2015

Kimmo Korhonen
Lasse Ahonen
Nicklas Nordbäck

Investigation of geological, geochemical and geothermal considerations related to geological intermediate storage of CO_2

ccsp
Carbon Capture and Storage Program

Cleen Ltd.
Research Report nr D413

Korhonen, Kimmo Lasse Ahonen and Nicklas Nordbäck

Investigation of geological, geochemical and geothermal considerations related to geological intermediate storage of CO_2

ccsp
Carbon Capture and Storage Program

Cleen Ltd
Helsinki 2015

Report Title: Investigation of geological, geochemical and geothermal considerations related to geological intermediate storage of CO_2

Key words: Carbon Dioxide, Intermediate CO_2 Storage, Geology, Geothermal, Geochemistry

Abstract

The Finnish bedrock is not suitable for the final storage of carbon dioxide (CO_2). However, it could be utilized as an intermediate storage medium. This document reports the investigation of geological, geochemical and geothermal considerations relating to the intermediate storage of CO_2 in a crystalline rock environment. The investigation was part of CCS WP 4.2.1 during FP4.

If shipping is used, the Carbon Capture and Storage (CCS) chain requires intermediate storage of CO_2. The conventional intermediate storage solution is steel tanks located above the ground. However, steel tanks may not be an economically viable solution to the intermediate storage of large amounts of CO_2. A better solution might be underground caverns in crystalline bedrock.

Storing CO_2 in liquid form could be carried out either at temperatures close to the ambient temperature of bedrock at higher CO_2 vapour pressures or at lower temperatures and lower CO_2 vapour pressures. Storage at ambient temperatures would require a confining water curtain to prevent the gas from leaking through fractured rock. However, storage at low temperatures (−40 °C) would naturally create an expanding frozen zone preventing leakage as frozen rock forms a rigid barrier that is impermeable to the gas.

Pure liquid CO_2 can be considered an inert phase towards the rock walls of a cavern store. The dissolution and diffusion of CO_2 in ice is negligible. On the other hand, CO_2 dissolves fairly well in water making a weak acid. These considerations favour the intermediate storage of CO_2 at low temperatures.

Finite Element Modelling indicates that storing CO_2 at the temperature of −40 °C in a rock cavern has a significant thermal effect on the bedrock. The temperature difference between the warm bedrock and the cold store induces a considerable heat flow towards the store during the first year of storage. Depending on store geometry, the magnitude of the heat flow peak is 1.2–1.5 MW (100-110 W/m^2). Once the bedrock in the vicinity of the store cools, the heat flow diminishes and approaches 80–120 W (7–9 W/m^2) after 100 years of storage. As the CO_2 needs to be kept constantly at the temperature of –40 °C, a considerable cooling capacity would be required.

Cooling the bedrock in the vicinity of the store before the actual storage of CO_2 would be advantageous and diminish the required cooling capacity. Using the capacity of 300 kW to cool the bedrock before storage for 9–20 months (depending on store geometry) would keep the required cooling capacity at 300 kW.

The modelling indicates that the most beneficial store geometry would be one that minimizes the cavern wall surface area. The depth of the store is also a factor that needs consideration. The temperature of bedrock increases downwards. This, stores located deeper would require more cooling. However, stores located at shallow depths would become susceptible to solar heating through the ground surface. The optimal location of the store is likely somewhere between 50 and 200 metres according to the results of thermal modelling.

The storage of cold liquid CO_2 in a rock cavern creates an expanding frozen zone and temperature disturbance. The cooling of the ground may become disruptive to constructs extending below the ground especially if the store is located at a shallow depth.

Helsinki, May 2015

Table of contents

1 Introduction

1.1 General

Carbon Capture and Storage (CCS) is based on the capture and liquefaction of carbon dioxide from industrial and combustion processes, on the transport of carbon dioxide to a storage site, and on the injection of carbon dioxide to geological storage formations. In order to permanently store carbon dioxide (CO_2), a porous and permeable geological formation with a caprock usually at depths below 800 m is needed. Porosity is required for the formation to store CO_2, permeability for the ability to inject large quantities of CO_2 into the formation, caprock to ensure that the injected CO_2 remains inside the formation, and sufficient depth to maximize the quantities stored (Chadwick et al., 2008).

The Finnish bedrock is composed mainly of crystalline and low porosity rock types which lack the potential to permanently store CO_2. The crystalline bedrock of Finland is part of the Precambrian Fennoscandian Shield, which was eroded down almost to its present level prior to the Cambrian (500 million years ago). Due to continental conditions and subsequent ongoing erosion, it is almost entirely lacking in sedimentary rocks younger than the Precambrian (Fig. 1).

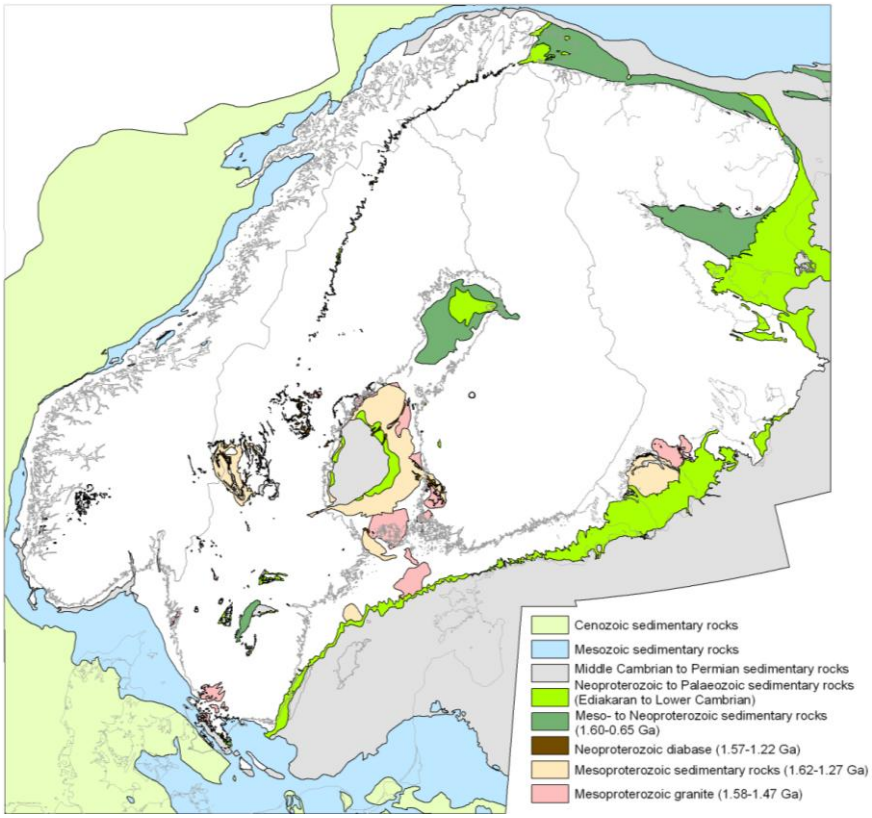

Figure 1. Sedimentary rocks of the Fennoscandian shield and the surrounding areas (Koistinen et al., 2001).

Finland has large CO_2 point sources, which are mainly located in coastal areas. Since Finland lacks the potential for permanent geological CO_2 storage, carbon dioxide captured in Finland would need to be transported and stored outside of the Finnish borders (Teir et al., 2011). The Norwegian continental shelf is especially abundant in potential geological storage sites, with the nearest operational CO_2 storage site (to Finnish point sources) also located in the Norwegian part of the North Sea. There is also some off-shore storage potential in the southern parts of the Baltic Sea (SLR, 2014) and on-shore storage potential in Latvia, Lithuania and the northern parts of Poland and Germany and in southern Denmark (Vangkilde-Pedersen et al., 2009).

Estimated costs of CO_2 transportation from Finnish point sources to final storage sites suggest that CO_2 transport by ship is the preferred transportation option over pipelines. Furthermore, joint transportation infrastructure and an increase in scale would decrease the transportation costs (Kujanpää et al., 2014). Shipping solutions require by default an intermediate storage for the captured CO_2. Conventionally intermediate storage facilities would be cylindrical steel tanks above the ground. However, rock caverns excavated deep below the ground could provide an alternative technology for intermediate CO_2 storage. Individual refrigerated cylindrical steel tanks are restricted in their size due to design demands. Thus, they do not have the same economic benefit from up scaling as underground caverns have. Preliminary results indicate that an underground storage unit of 50,000 m^3 or larger would have a significantly smaller investment costs than a steel tank storage complex of the same size (Ritola et al., 2014).

While the compact and dense Scandinavian bedrock is not suitable for final storage of CO_2, it could be particularly suitable for intermediate storage. The design of an intermediate underground CO_2 storage facility would be analogous to a refrigerated LNG or LPG gas store in unlined rock caverns. Existing technology and experience from LPG (and small scale CO_2) transport and storage could also be transferred to liquid transport CO_2 infrastructure. The most essential issue associated with underground oil and gas storage is the prevention of leaking of gas and oil from storage caverns. In the case of intermediate CO_2 rock cavern storage, frozen groundwater could be used as a seal to make the rock mass impermeable.

This report presents the work carried out during the fourth funding period (FP4) of task 4.2.1 of the Carbon Capture and Storage Programme (CCSP). This task will be continued in 2015. The results presented in this report include geological, geothermal and geochemical considerations related to the intermediate CO_2 rock cavern storage concept and preliminary results from thermal modelling.

1.2 Liquid CO_2 and its interaction with rocks

The liquid form of carbon dioxide provides the best properties in terms of volume and transferability of the material. Liquid CO_2 is stable at pressures above 10 bars at −40 °C, with pressure gradually increasing to about 40–50 bar at temperatures approaching the ambient temperatures of the Finnish bedrock.

The equilibrium condition between the liquid and gaseous forms of CO_2 is defined by the vapour pressure or, more precisely, fugacity of CO_2. The vapour pressure of liquid CO_2 is between the vapour pressures of methane (LNG) and propane (LPG) (Fig. 2). If cooler than the environment, liquid carbon dioxide will boil until the equilibrium pressure is attained. A prerequisite for the

containment of CO_2 inside an intermediate store is that the walls are impermeable to the gas pressure and/or that the pressure outside the storage exceeds the vapour pressure inside.

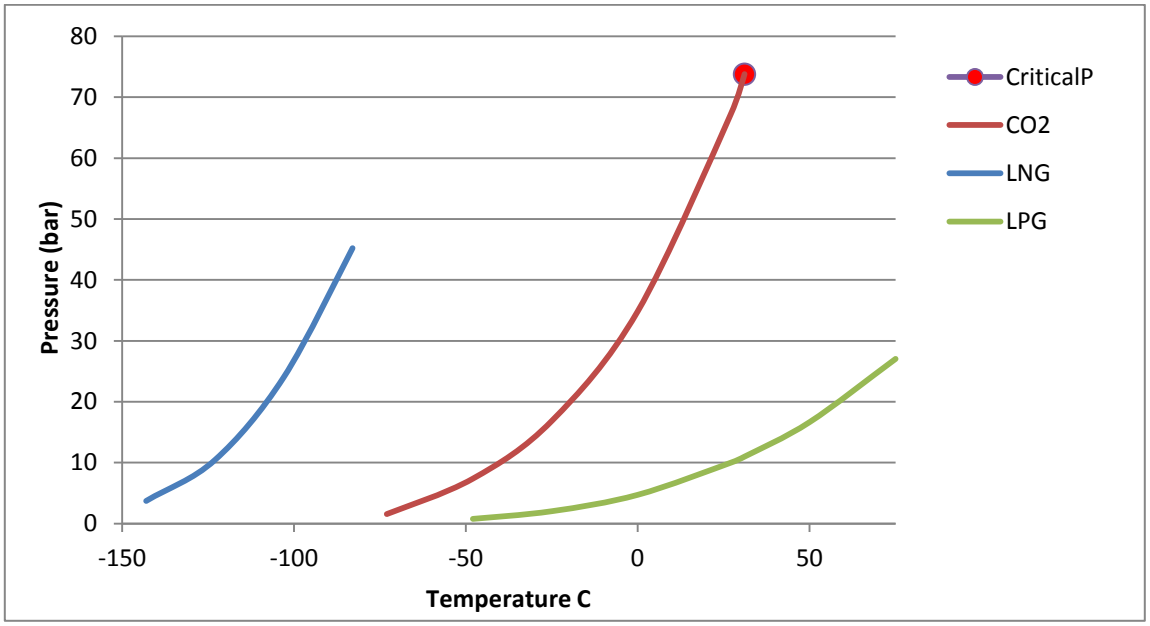

Figure 2. Equilibrium vapour pressure of liquid LNG, CO_2 an LPG as a function of temperature.

Close analogues to CO_2 with respect to rock storage are the liquefied hydrocarbons methane and ethane (liquid natural gas, LNG, and liquid petroleum gas, LPG, respectively). Due to the high vapour pressure, LNG requires extremely low temperature and good thermal insulation of the storage whereas the relatively low vapour pressure of LPG makes it ideal for rock storage at ambient temperatures.

Compared to the hydrocarbons LPG and LNG, a CO_2 molecule dissolves fairly well in water. On the other hand, dissolution of CO_2 in ice is negligible, as well as the diffusion of CO_2 in ice. Diffusion studies of CO_2 in gas bubbles in Antarctic ice cores have shown excellent preservation of the original gas phase at time scales of hundreds of thousands years (Ahn et al., 2008).

Interaction between liquid CO_2 and a rock wall would be a potential source of impurities in the liquid phase. The pure liquid form of CO_2 can be considered as an inert phase towards the solid rock surface. However, the phase boundary may also include micro-environments where ice and the CO_2 vapour phase interact. In principle, molecular CO_2 and water together form a carbonic acid molecule (H_2CO_3) which in liquid water reacts as a weak acid releasing a proton and a bicarbonate molecule (HCO_3^-). Acidification has the tendency to dissolve carbonate minerals in rocks. Bateman et al. (2013) reported a 5-year experimental study on the interactions between supercritical CO_2 (80 bar, 30 °C) and clay-rich, slightly carbonaceous (2.4% calcite) Utsira caprock from the Sleipner gas field. Their results indicate the release of Ca from calcite dissolution, but no other clear mineralogical changes, even though the liquid phase of water was present.

1.3 Storage principles

The starting point of the present report is the storage of liquid CO_2 at temperatures around −40 °C. This would keep the CO_2 volume and vapour pressure low (Ritola et al., 2014). The low temperature of the CO_2 liquid would further facilitate its own containment by forming a frozen zone around the store. Within this zone, water in fractures would remain frozen which would prevent the CO_2 from escaping the store. However, heat flow from the warmer bedrock to the colder store would become a major issue.

Another storage option is to keep the storage temperature close to the ambient conditions, which in Southern Finland means temperatures of 6–8 °C depending on depth. On the other hand, an impermeable frozen zone around the CO_2 store is required. A confining over-pressurized water curtain would allow the mixing of liquid water and carbon dioxide. Consequently, the upper end of the relevant temperature range for liquid CO_2 storage is a few degrees below zero, i.e., the freezing temperature of water. This would decrease the heat flow, whereas the thickness of the frozen zone might become a critical factor.

Provided that the frozen zone surrounding the storage is essentially rigid and impermeable for gas, vapour pressure of liquid CO_2 will control the pressure within the store. Absorption of thermal energy from the surroundings tends to increase the vapour pressure of CO_2 in a closed system. Consequently, temperature-pressure conditions during storage tend to evolve along the vapour pressure curve shown Fig. 2 (the red curve), i.e., along the liquid/gas phase boundary of Fig. 3.

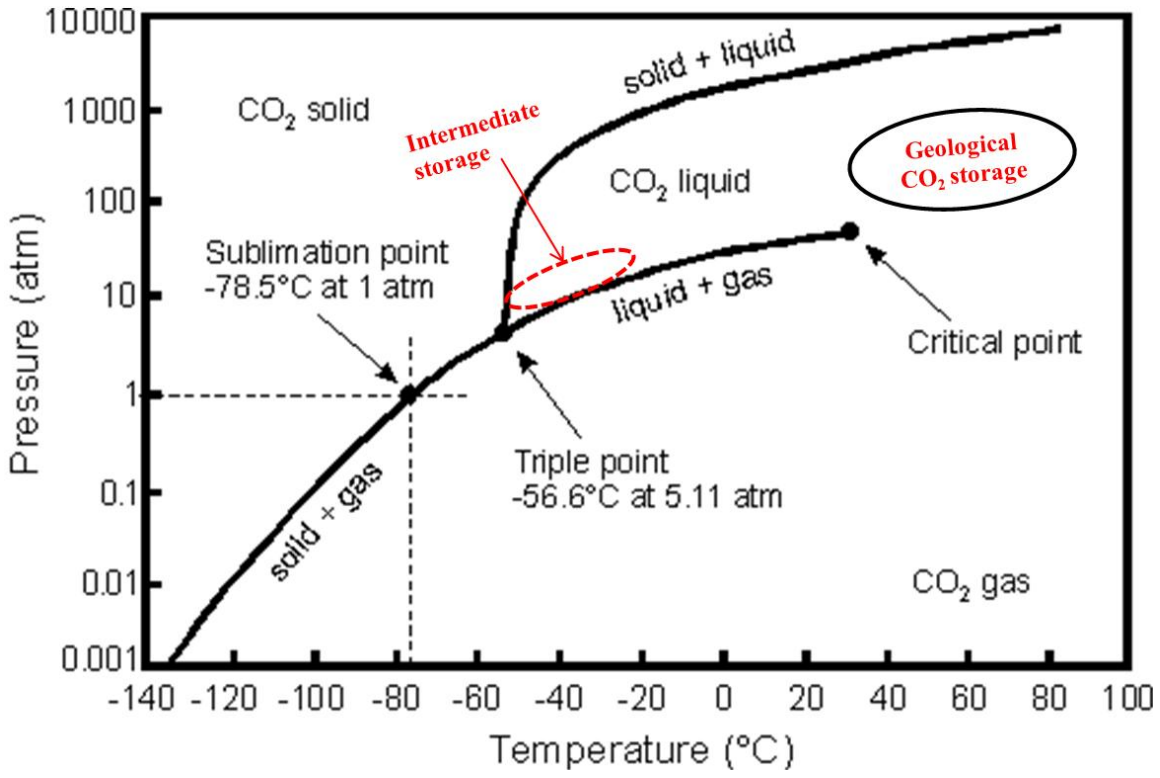

Figure 3. Phase diagram of CO_2.

1.4 Permeability of frozen rock

One of the fundamental factors controlling the behaviour of a cavern in frozen-rock is the permeability of the rock-ice system. Crystalline rocks contain free water mainly in open fractures of different scales. In addition to the free water, some water may be electrostatically bound to clay-bearing rock gouge, which may have some permeability at temperatures below the freezing point of free water. Observations from the Lupin Mine below the base of permafrost indicate that a thick layer of frozen rock forms an essentially rigid and impermeable barrier (Fig. 4).

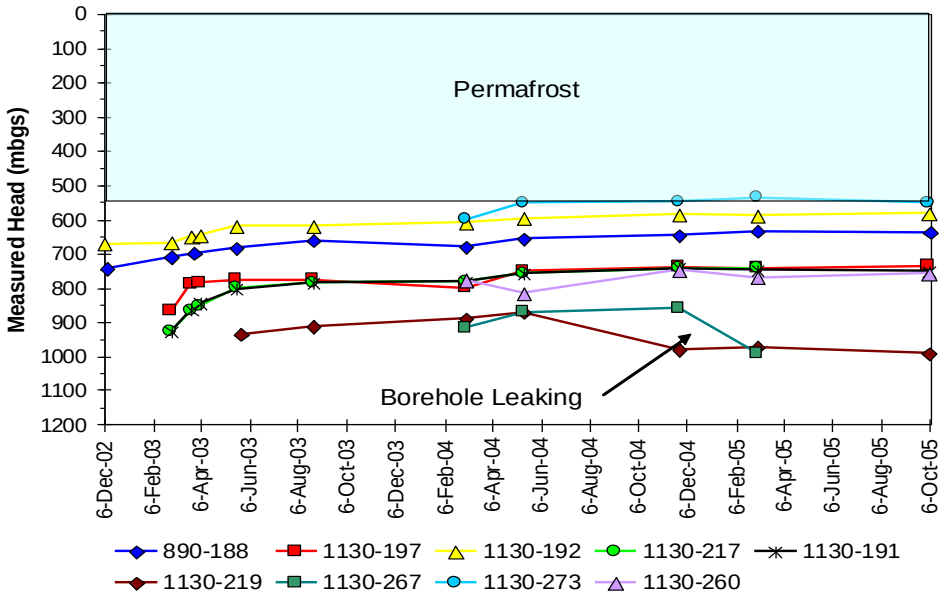

Figure 4. Hydraulic permeability of frozen bedrock. Maximum hydrostatic pressures below the deep permafrost were controlled by the base of the frozen zone above.

1.5 Site selection for the thermal modelling of an intermediate CO_2 store

Ritola et al. (2014) considered three potential sites for intermediate CO_2 storage. One of these sites was selected for the thermal modelling presented in this report. The Kilpilahti site is located in the city of Porvoo in Southern Finland. The geology of Kilpilahti is characterized by granites as is evident from the lithological map presented in Fig. 5.

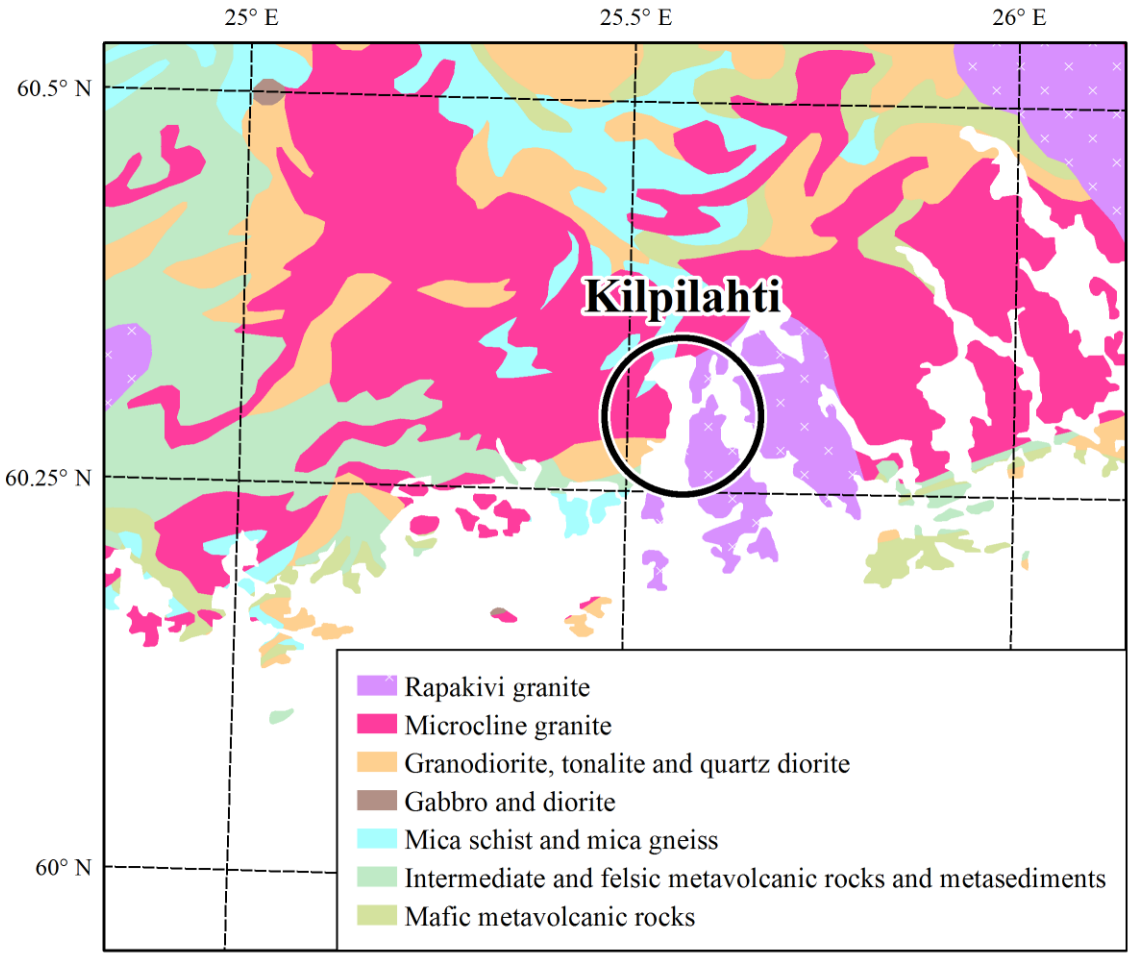

Figure 5. *Lithological map of Porvoo, Southern Finland (copyright Gelogical Survey of Finland).*

1.6 Conceptual model and simulation scenarios

For modelling purposes, the system was defined as follows. A store of 50,000 m^3 capacity was sited deep below the ground surface within a homogeneous and isotropic granitic rock unit. The surface was assumed to remain exposed throughout the year so that the effect of snow could be neglected. The bedrock was assumed to be porous and fully saturated with groundwater. However, the groundwater was assumed to remain immobile so that convection of heat could be neglected. Thus, heat transfer was assumed to occur purely by conduction. The pore-filling groundwater was assumed to freeze and thaw when temperatures dropped below zero centigrades and rose above zero centigrades respectively. The rocks were assumed to contain radioactive elements that produced heat and the geothermal heat flux was assumed to be in effect.

The storage pressure and temperature were chosen to be 10 bars and −40 °C respectively. Storing a liquid this cold directly in warm bedrock would induce a large heat flow into the store during the beginning of the storage period because the initial thermal gradient would be nearly 50 kelvins. Because the stored CO_2 needs to be kept constantly at −40 °C, a considerable cooling capacity

would be required. To reduce the required cooling capacity, it might be advantageous to first cool the bedrock in the vicinity of the store. Thus, the following two simulation scenarios were considered.

1. Storage of liquid CO_2 directly in warm bedrock without an initial cooling period.
2. Storage of liquid CO_2 in bedrock after an initial cooling period during which the bedrock in the vicinity of the intermediate store is cooled using a cooling power of 300 kW until the average cavern wall temperature has dropped to −40 °C.

2 Finite element thermal model

2.1 Model geometry

Two store geometries were modelled (Fig. 6). The ***single cavern store*** consisted of a single long cavern while the ***dual cavern store*** consisted of two shorter caverns running in parallel. The geometry of the cavern cross section and the parameters defining it are shown in Fig. 7. The area of the cross section is

$$A = \frac{W_{\mathrm{roof}} + W_{\mathrm{floor}}}{2} \cdot \left(H - H_{\mathrm{roof}}\right) + \frac{\pi \cdot W_{\mathrm{roof}} \cdot H_{\mathrm{roof}}}{4} . \quad (1)$$

Two cavern cross sections of different sizes were considered. The small and large cross sections. The geometrical parameters of these cross sections are listed in Table 1. The lengths and resulting nominal volumes of all the four modelled store geometries are listed in Table 2. The cavern separation for the dual cavern models was chosen to be 35 m.

Table 1. *Geometrical parameters of store cross sections.*

Cross section	W_{floor} [m]	W_{roof} [m]	H_{roof} [m]	H [m]	A [m^2]
Small	18	14	2.2	22	341
Large	18	16	3.6	35	579

Table 2. *Modelled stores with caverns lengths and resulting store volumes.*

Store geometry	Cross section	L [m]	V [m^3]
Single cavern	Small	170	57970
Single cavern	Large	100	57900
Dual cavern	Small	85	57970
Dual cavern	Large	50	57900

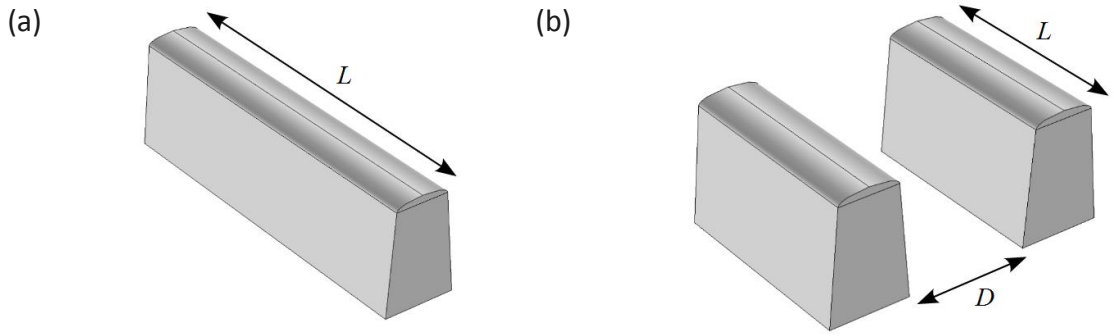

Figure 6. *Modelled store geometries. (a) The single cavern store. (b) The dual cavern store. L is the length of the caverns. D is the cavern separation.*

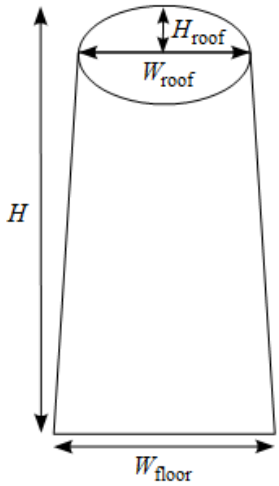

Figure 7. *Geometry of the cavern cross section. The cross section is formed as a union of an isosceles trapezoid and an ellipsoid. The top and the base of the trapezoid have lengths W_{roof} and W_{floor} respectively. The minor radius and major axis of the roof ellipsoid are H_{roof} and W_{roof} respectively.*

The modelled store geometries were not long enough to warrant 2-D modelling. Heat transfer due to the ends of the caverns also had to be taken into account because it had a significant influence on the total heat transfer. Thus, 3-D models of each of the four store geometries (Table 2) were constructed.

The modelled store geometries contained two symmetry planes through which heat flow did not occur. These symmetry planes are illustrated in Fig. 8. Due to the symmetries, only a single quadrant of the complete 3-D model needed to be modelled (Fig. 8).

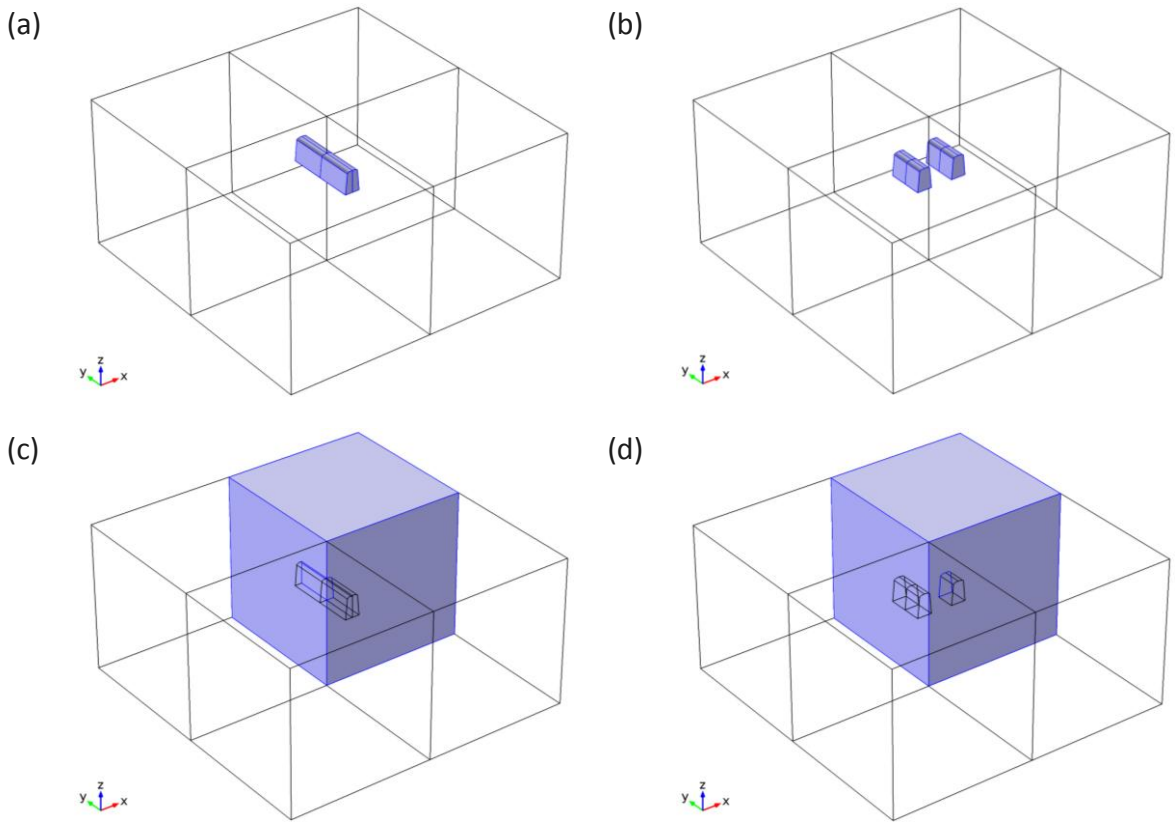

Figure 8. *Schematic illustration of the symmetries exploited in the modelling. The complete 3-D model geometries for the (a) single and (b) dual cavern store geometries. Both models feature two symmetry planes that intersect at the centre. These are the XZ and YZ planes intersecting at the centres of the models. No heat flows through these planes. Thus, only a quadrant of the complete 3-D model geometry needs to be considered. The quadrants chosen for modelling the (c) single and (d) dual cavern stores. The scaling is exaggerated.*

The 3-D models consisted of a single continuous bedrock domain. The caverns itself were carved out of the bedrock domain using the difference operation of constructive solid geometry because the effect of CO_2 storage could be modelled using boundary conditions only (Fig. 9).

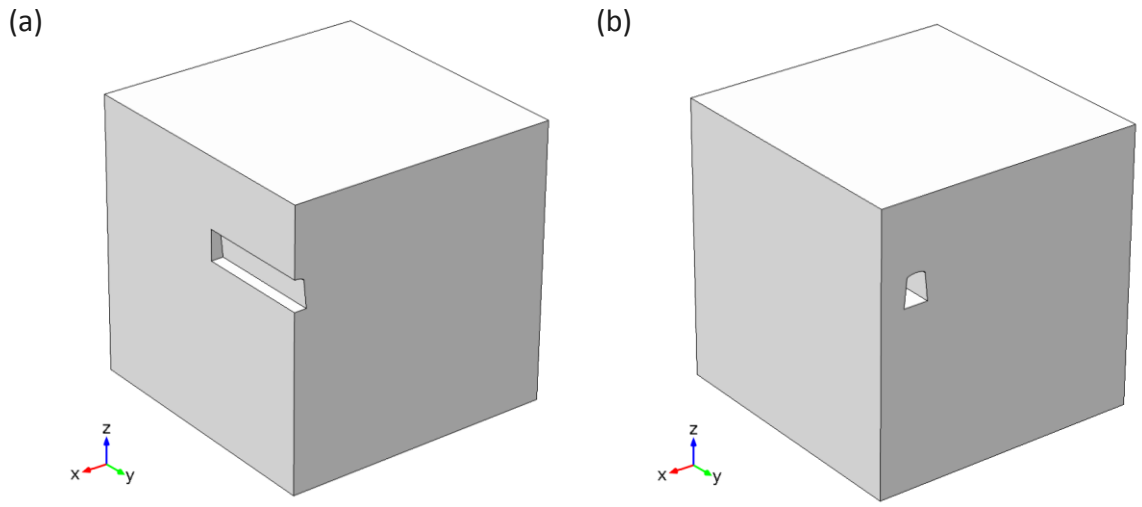

Figure 9. *Schematic illustration of the 3-D model geometries. (a) The single cavern model. (b) The dual cavern model. The scaling is exaggerated.*

2.2 Computational mesh

Finite element meshes of the modelled geometries were generated from tetrahedral and prismatic elements. Fig. 10 shows an example of the computational mesh for one model. The top-most 20 meters of the models were meshed using prismatic elements of 1 meter height in order to resolve the annual temperature variations adequately (see Fig. 10a). The immediate surroundings of the caverns were meshed using tetrahedral elements with a maximum side length of 1 meter in order for the heat flux calculations to be accurate (see Fig. 10b). Furthermore, a refinement zone around the caverns was created in order to resolve temporal and spatial changes properly (see Fig. 10b).

(a)

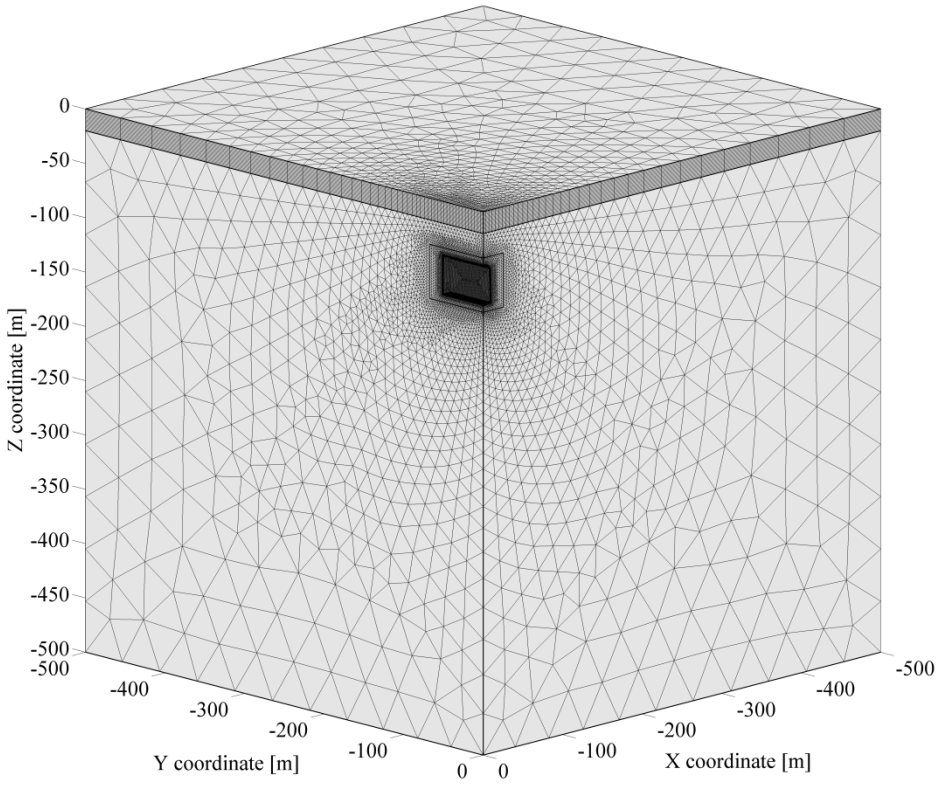

(b)

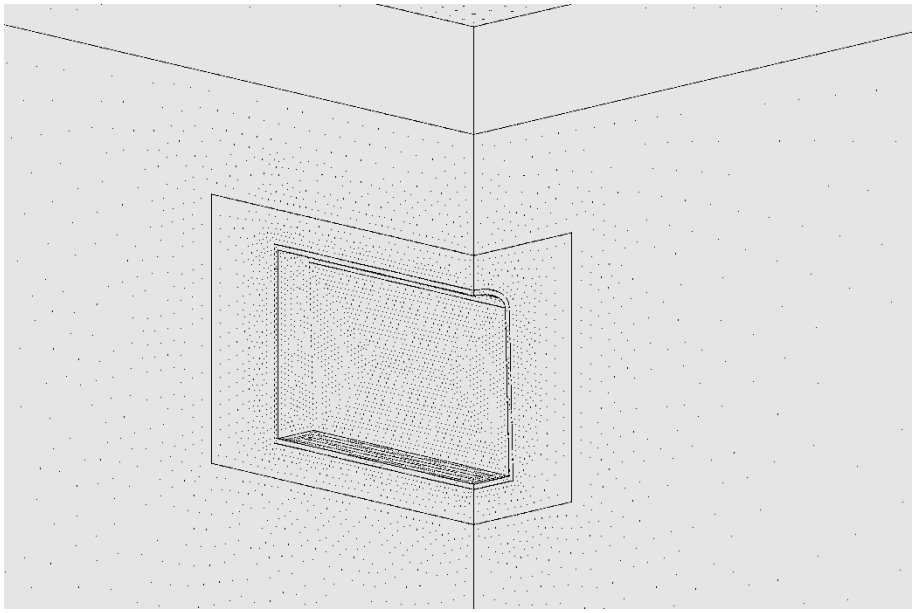

Figure 10. *Illustration of the computational mesh. (a) The computational mesh of the single cavern model located at the depth of 50 m. (b) A close up of the mesh.*

2.3 Modelled physics

2.3.1 Governing equation

Heat transfer was assumed to be purely conductive. The partial differential equation describing conductive heat transfer is

$$\rho \cdot C_p \cdot \frac{\partial T}{\partial t} = \nabla \cdot (k \cdot \nabla T) + Q_{\text{radiogenic}}, \quad (1)$$

where ρ is density, C_p is specific heat capacity at constant pressure, T is temperature, t is time, k is thermal conductivity and $Q_{\text{radiogenic}}$ is the radiogenic heat production. Because the bedrock was assumed to be porous, the material properties used in Eq. (1) were modelled as equivalent properties defined as the volumetric averages

$$k = (1-\theta) \cdot k_{\text{granite}} + \theta \cdot k_{\text{groundwater}} \quad (2)$$

and

$$\rho \cdot C_p = (1-\theta) \cdot \rho_{\text{granite}} \cdot C_{p,\text{granite}} + \theta \cdot \rho_{\text{groundwater}} \cdot C_{p,\text{groundwater}}, \quad (3)$$

where θ is the liquid fraction (porosity), $1-\theta$ is the solid fraction, k_{granite} and $k_{\text{groundwater}}$ are the thermal conductivities of the granitic bedrock and the pore-filling groundwater respectively, and $\rho_{\text{granite}} \cdot C_{p,\text{granite}}$ and $\rho_{\text{groundwater}} \cdot C_{p,\text{groundwater}}$ are the volumetric heat capacities of the bedrock and groundwater respectively.

2.3.2 Phase change

The bedrock was assumed to be porous and fully saturated. When the temperature of the rock matrix drops below zero, the groundwater that fills the pores starts to freeze. During the phase change from water to ice, the thermal conductivity, specific heat capacity and density of groundwater change. These physical properties were modelled using

$$k_{\text{groundwater}} = (1-\alpha) \cdot k_{\text{ice}} + \alpha \cdot k_{\text{water}}, \quad (4)$$

$$C_{p,\text{groundwater}} = (1-\alpha) \cdot C_{p,\text{ice}} + \alpha \cdot C_{p,\text{water}} + L_{\text{fusion}} \cdot \frac{\mathrm{d}\alpha}{\mathrm{d}T} \quad (5)$$

and

$$\rho_{\text{groundwater}} = \frac{(1-\alpha) \cdot C_{p,\text{ice}} \cdot \rho_{\text{ice}} + \alpha \cdot C_{p,\text{water}} \cdot \rho_{\text{water}}}{(1-\alpha) \cdot C_{p,\text{ice}} + \alpha \cdot C_{p,\text{water}}}, \quad (6)$$

where α is a function of temperature and gives the fraction of the water phase inside the pores, $1-\alpha$ gives the fraction of the ice phase inside the pores, L_{fusion} is the latent heat of fusion of water (333 kJ/kg), k_{ice} and k_{water} are the thermal conductivity of ice and water respectively, $C_{p,ice}$ and $C_{p,water}$ are the specific heat capacity of ice and water respectively, and ρ_{ice} and ρ_{water} are the density of ice and water respectively (COMSOL, 2013b). The value of the α function was assumed to change smoothly from 0 to 1 when temperature rises from $273.15-\Delta T/2$ K to $273.15+\Delta T/2$ K, where ΔT is the width of the transition zone which was chosen to be 1 kelvin.

2.4 Boundary conditions

Five different boundary conditions were applied to the model boundaries. Fig. 11 illustrates these boundary conditions and the boundaries to which they were applied.

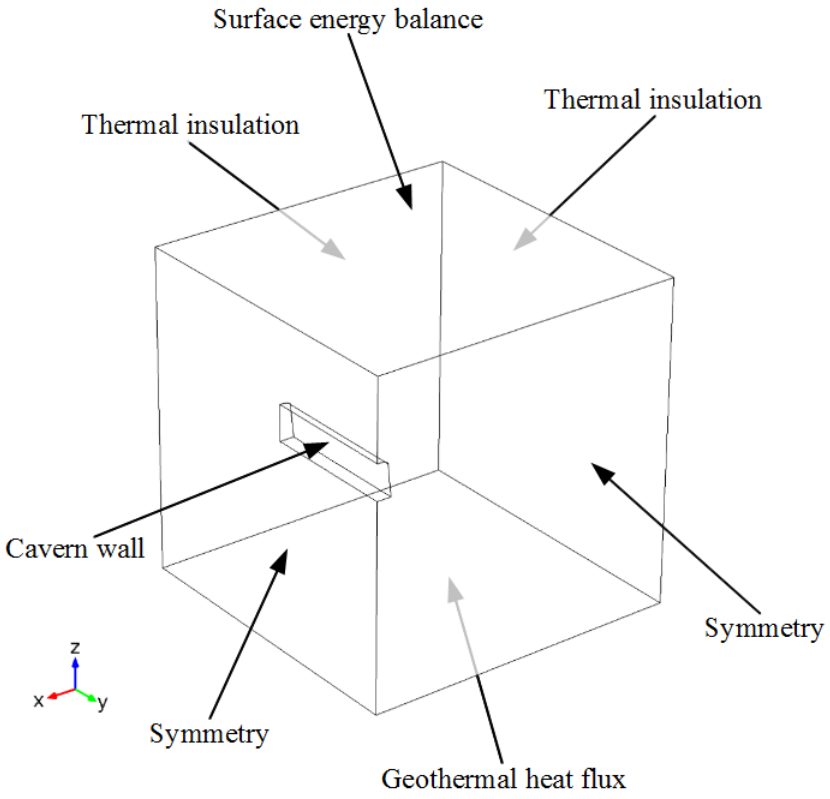

Figure 11. *Boundary conditions applied. Heat flux boundary conditions were applied to the top and bottom boundaries. The heat flux through the top surface was calculated based on the ground surface energy balance equation. The geothermal heat flux was used as the heat flux through the bottom boundary. The vertical boundaries were applied either thermal insulation or symmetry boundary conditions. The cavern walls were applied either heat flux boundary condition (during the cooling period) and/or constant temperature boundary condition (during the storage period).*

2.4.1 Boundary condition on the top surface

The top surfaces of the models were assigned the outward heat flux boundary condition

$$-k \cdot \frac{\partial T}{\partial z} = G\,, \tag{7}$$

where G is the conductive heat flux from the ground into the atmosphere. It was calculated on the basis of the ground surface energy balance equation

$$R_{\text{net}} = G + H + L_{\text{vapour}} \cdot E\,, \tag{8}$$

where R_{net} is the net radiation incident on the ground surface, H is the turbulent sensible heat flux and $L_{\text{vapour}} \cdot E$ is the turbulent latent heat flux (L_{vapour} is the latent heat of vaporization of water, 2245 kJ/kg, and E is evaporation from the ground surface) (e.g., Deardorff, 1978).

The net radiation was given by

$$R_{\text{net}} = (1 - \text{albedo}) \cdot Q_{\text{solar}} + \varepsilon_{\text{ground}} \cdot (Q_{\text{atmosphere}} - \sigma \cdot T_{\text{ground}}^4)\,, \tag{9}$$

where Q_{solar} is the incoming solar radiation, albedo is the ratio of reflected to absorbed solar radiation at the ground surface, $\varepsilon_{\text{ground}}$ is the emissivity of the ground surface, $Q_{\text{atmosphere}}$ is the thermal radiation emitted by the atmosphere, σ is the Stefan-Boltzmann constant ($5.670373 \cdot 10^{-8}$ W/m^{2}K^4) and T_{ground} is the ground temperature (e.g., Deardorff, 1978). The sensible heat flux was modelled using

$$H = h \cdot (T_{\text{ground}} - T_{\text{air}})\,, \tag{10}$$

where T_{air} is the air temperature and h is the turbulent convective heat transfer coefficient which was estimated using the linear correlation $h = 5.8 + 4.1 \cdot v_{\text{mean}}$, where v_{mean} is the mean wind velocity (e.g., Fujii et al., 2012).

2.4.2 Boundary condition on the bottom surface

The bottom surface was assigned the inward heat flux boundary condition

$$k \cdot \frac{\partial T}{\partial z} = q_{\text{geo}}\,, \tag{11}$$

where q_{geo} is the geothermal heat flux into the model domain.

2.4.3 Boundary conditions on the vertical surfaces

The vertical surfaces were assigned either symmetry or thermal insulation boundary conditions. These boundary conditions are equivalent to the adiabatic or no-flux boundary condition

$$k \cdot \frac{\partial T}{\partial n} = 0\,, \tag{11}$$

where *n* is the direction normal to the surface (either the *x* or *y* direction).

2.4.4 Cavern wall boundary conditions

In simulations containing only a storage period, the cavern walls were assigned the temperature boundary condition. In these simulations, the cavern wall temperature was gradually decreased from the initial bedrock temperature to the storage temperature of −40 °C during the first simulated month. This was necessary in order to avoid large temperature gradients at the cavern walls that would have caused numerical problems.

In simulations containing both an initial cooling period and a storage period, two different boundary conditions were applied on the cavern walls. In the beginning of the cooling period, the cavern walls were assigned the heat flux boundary condition

$$-\mathbf{n} \cdot (-k \cdot \nabla T) = -\frac{Q_{\text{cooling}}}{A_{\text{walls}}}\,, \tag{11}$$

where **n** is the outward unit normal to the boundary, Q_{cooling} is the cooling capacity and A_{walls} is the surface area of the cavern walls. The heat flux due to the cooling was gradually increased from 0 to its full value during the first month of the cooling period in order to avoid numerical problems. Then, in the beginning of the storage period, the boundary condition was changed to the constant temperature boundary condition which was used to set the cavern wall temperature to −40 °C for the rest of the simulation.

2.5 Initial ground temperature profile

The initial ground temperature profile for the simulations was calculated using a 1-D model that was equivalent to the 3-D model in all aspects but disregarding the carbon dioxide store. The 1-D model was initialized with an arbitrary temperature distribution and was ran until a balance was reached between the geothermal and surface heat fluxes. The resulting temperature distribution for the 1st of January (Fig. 12) was used to initialize the temperatures in the 3-D simulations.

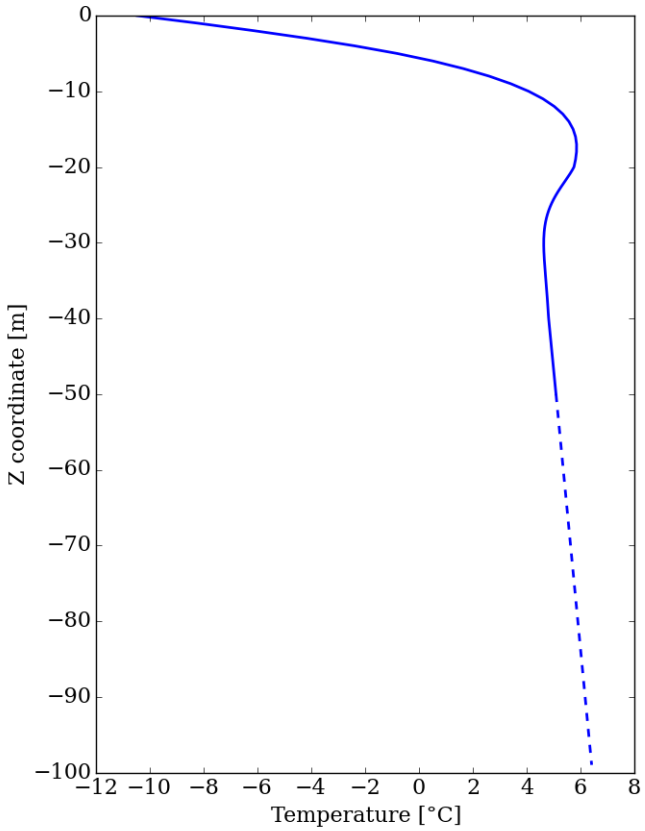

Figure 12. *Initial temperature profile for the 3-D carbon dioxide store simulations.*

2.6 Functions and parameter values used in modelling

Periodical functions were devised for solar radiation, atmospheric radiation, air temperature, albedo and ground emissivity for use in the ground surface boundary condition given in Eqs. (8)–(10). The functions are of the general form

$$f(t) = A \cdot \sin(\omega \cdot t + \varphi) + c\,, \tag{12}$$

where A is the amplitude, ω is the angular frequency of one year ($2 \cdot \pi / 365.2425 \cdot 86400$ 1/s), φ is the phase offset and c is a coefficient. The parameters A, φ and c were estimated by fitting a function of the form of Eq. (12) to data using the Levenberg-Marquardt optimization method.

The solar radiation, atmospheric radiation and air temperature functions were based on data obtained for the store location (latitude 60.5 °N and longitude 25.5 °E) from the Surface and Solar Energy (SSE) web portal (supported by the NASA LaRC POWER Project) of the Atmospheric Science Data Center of NASA Langley Research Center (https://eosweb.larc.nasa.gov/cgi-bin/sse/sse.cgi). Fitting Eq. (12) to data resulted in the functions

$$Q_{\text{solar}} = 117.408 \cdot \sin(\omega \cdot t + 4.930) + 117.408\,, \tag{13}$$

$$Q_{\text{atmosphere}} = 52.299 \cdot \sin(\omega \cdot t + 4.302) + 284.525 \tag{14}$$

and

$$T_{\text{air}} = 12.243 \cdot \sin(\omega \cdot t + 4.365) + 4.097 \tag{15}$$

(see Figs. 13– 15).

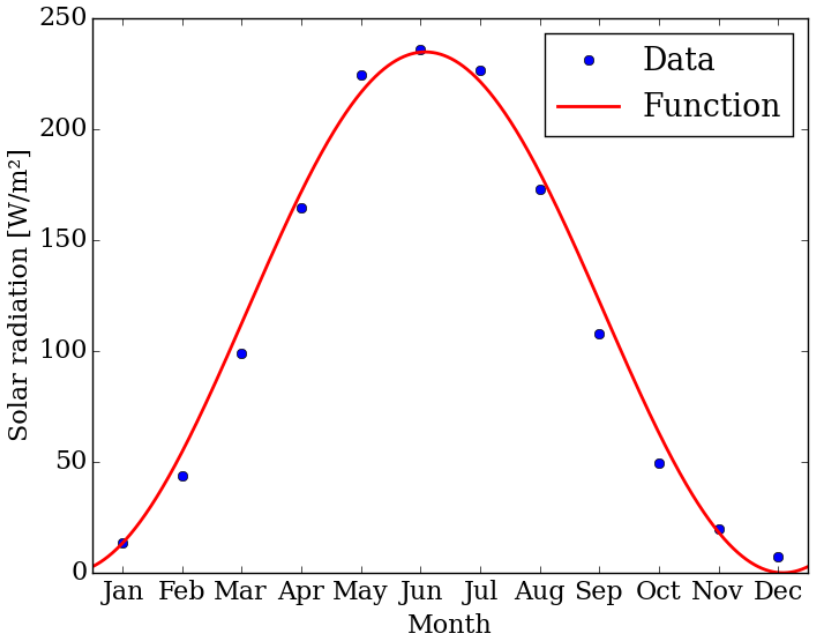

Figure 13. *Solar radiation data and function used in the ground surface boundary condition.*

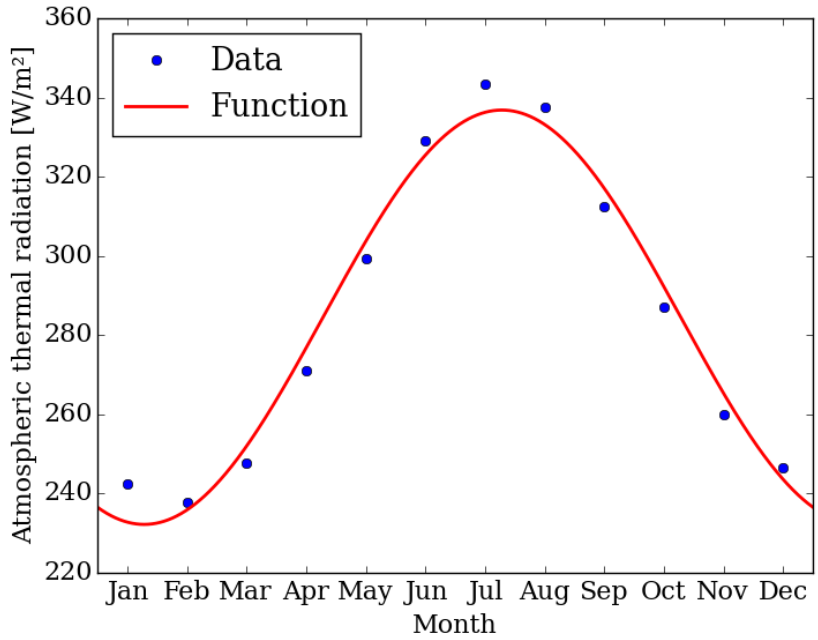

Figure 14. *Atmospheric radiation data and function used in the ground surface boundary condition.*

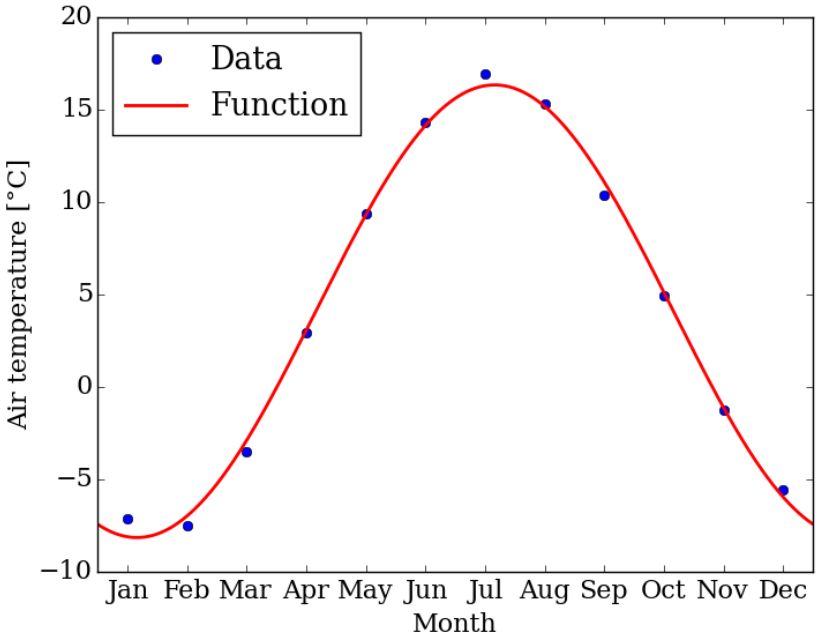

Figure 15. *Air temperature data and function used in the ground surface boundary condition.*

The albedo function was based on data obtained for Jokioinen, Southern Finland, which is a location close to the modelled store location. The data was obtained from the Global Energy Balance Archive (http://www.geba.ethz.ch/) (Gilgen and Ohmura, 1999) of the Swiss Federal Institute of Technology in Zurich. Fitting a modified version of Eq. (12) to the data resulted in the function

$$\text{albedo} = \max(0.125 \cdot \sin(\omega \cdot t + 0.572) + 0.092,\ 0.092) \tag{16}$$

(see Fig. 16). Because the albedo is fairly constant during the summer and early autumn, the sinusoidal function of Eq. (12) was modified to better incorporate this property of the annual albedo variation by not allowing albedo values below 0.092 using the max function.

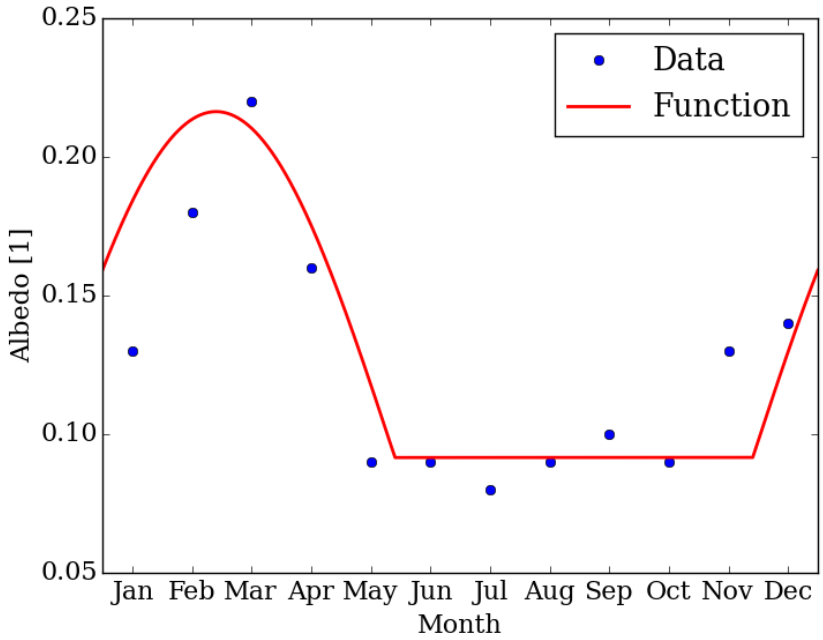

Figure 16. *Albedo data and function used in the ground surface boundary condition.*

The ground emissivity function was based on data for the modelled store location (latitude 60.5 °N and longitude 25.5 °E) obtained from the University of Wisconsin-Madison Baseline Fit Emissivity Database (http://cimss.ssec.wisc.edu/iremis/) (Seeman et al., 2007). Fitting Eq. (12) to the data resulted in the function

$$\varepsilon_{\text{ground}} = 0.009 \cdot \sin(\omega \cdot t + 0.399) + 0.976 \tag{17}$$

(see Fig. 17).

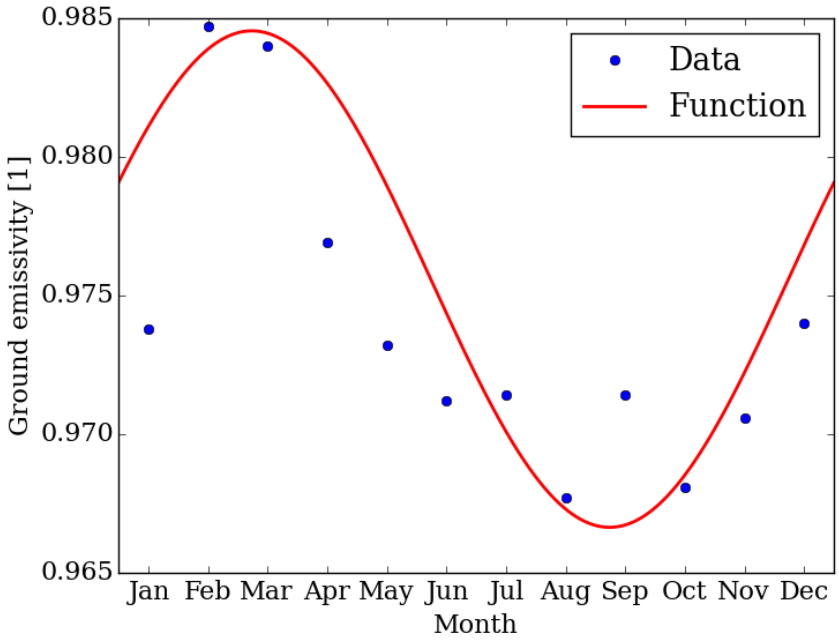

Figure 17. *Ground emissivity data and function used in the ground surface boundary condition.*

Parameter values used in Finite Element modelling and simulations are listed in Table 3. The mean wind speed and average annual precipitation were based on meteorological data obtained for the modelled store location (latitude 60.5 °N and longitude 25.5 °N) from the NASA SSE web portal.

Table 3. *Parameter values used in Finite Element modelling and simulation.*

Parameter (symbol)	Value
Width of model domain	500 m
Height of model domain	500 m
Geothermal heat flux (q_{geo})	50 μW/m^2 [a]
Radiogenic heat production ($Q_{radiogenic}$)	1.35 mW/m^3 [b]
Mean wind speed (v_{mean})	3.047 m/s
Heat transfer coefficient ($h = 5.8 + 4.1 \cdot v_{mean}$)	18.293 W/(m^{2}K)
Thermal conductivity of bedrock (k_{rock})	3.71 W/mK [b]
Specific heat capacity of bedrock ($C_{p,rock}$)	698 J/kgK [c]
Density of bedrock (ρ_{rock})	2645 kg/m^3 [b]
Thermal conductivity of water (k_{water})	0.57 W/mK
Specific heat capacity of water ($C_{p,water}$)	4180 J/kgK
Density of water (ρ_{water})	1000 kg/m^3
Thermal conductivity of ice (k_{ice})	2.22 W/mK
Specific heat capacity of ice ($C_{p\ ice}$)	2050 J/kgK
Density of ice (ρ_{ice})	916 kg/m^3
Porosity of bedock (θ)	0.5 %
Average annual precipitation (p_{annual})	587 mm/a
Evaporative heat flux ($E = \rho_{water} \cdot L_{vapour} \cdot p_{annual}$)	41.759 W/m^2
Cooling power ($Q_{cooling}$)	300 kW

[a] Kukkonen (1989)
[b] Peltoniemi and Kukkonen (1997)
[c] Kukkonen et al. (2011)

3 Results of thermal modelling

The temperature evolution of the bedrock was simulated for a 100-year time period. Simulations with and without an initial cooling period were ran for the single and dual cavern models of small and large cavern cross sections located at 50-m, 100-m and 200-m depths. This resulted in 24 simulations altogether. The lengths of the cooling periods for the simulations containing an initial cooling period are listed in Table 4.

Table 4. *Lengths of the initial cooling periods for simulations containing an initial cooling period.*

Store model	Cavern cross section	Store depth [m]	Cooling period in months
Single cavern	Small	50	14
Single cavern	Small	100	15
Single cavern	Small	200	16
Single cavern	Large	50	9
Single cavern	Large	100	9
Single cavern	Large	200	10
Dual cavern	Small	50	18
Dual cavern	Small	100	19
Dual cavern	Small	200	20
Dual cavern	Large	50	13
Dual cavern	Large	100	13
Dual cavern	Large	200	14

Fig. 18 illustrates the magnitudes of heat flows and heat fluxes through the cavern walls during the simulations. The heat flow through the cavern walls was calculated as

$$Q_{\text{walls}} = 4 \cdot \int_{\partial\Omega} \mathbf{q} \cdot \mathbf{n} \, \mathrm{d}s \tag{18}$$

where $\partial\Omega$ is the cavern wall surface, **q** is the heat flux vector through the surface and **n** is the outward unit normal vector to the surface. Multiplication by four was required since the model contained only a quadrant of the complete 3-D geometry. Heat fluxes were calculated by dividing the heat flows by the effective surface areas of the cavern walls (Table 5).

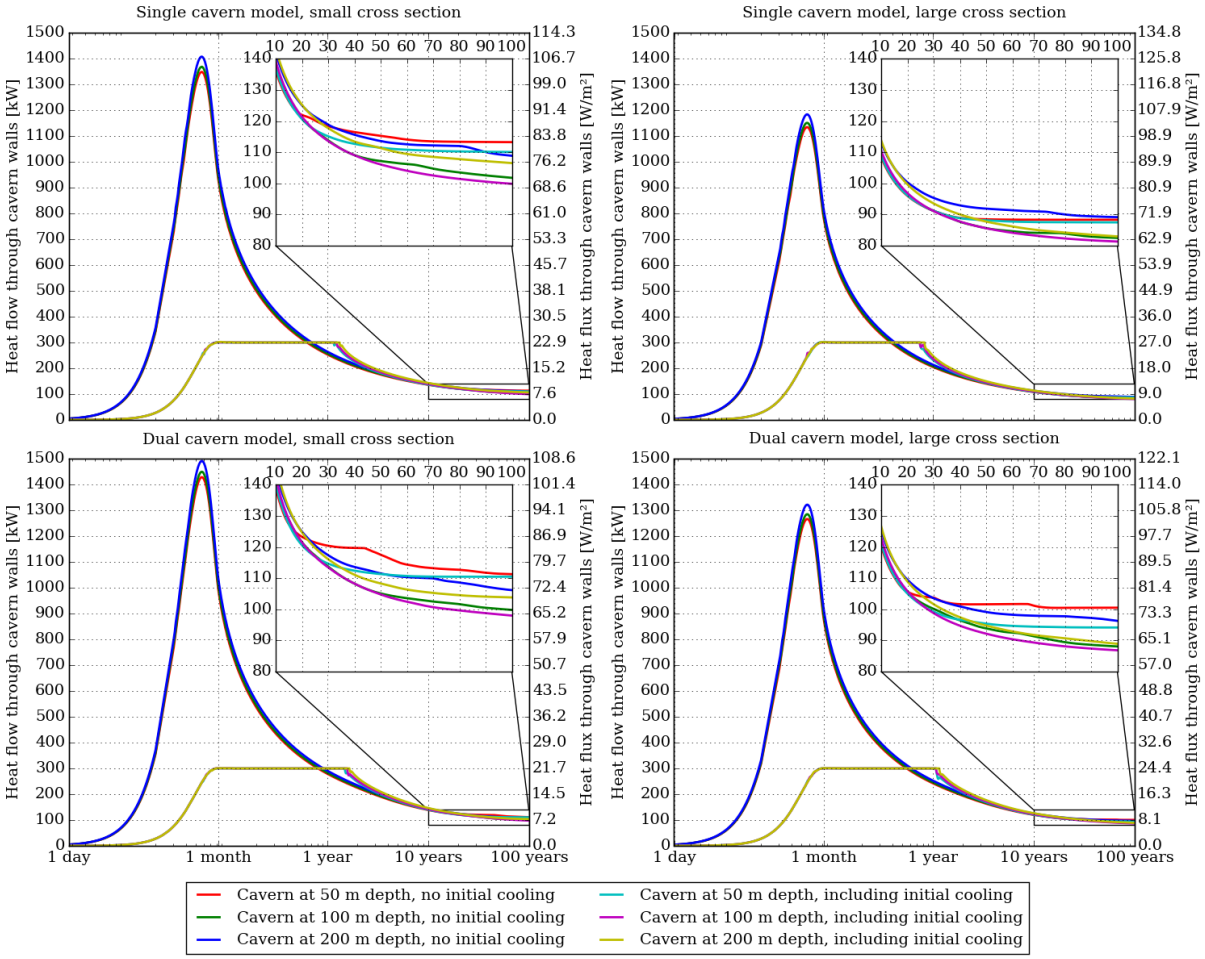

Figure 18. *Heat flows and heat fluxes through the cavern walls in all 24 simulations. The insets show zoomed portions of the temporal evolution of heat flow in each simulation for the last 90 years.*

Table 5. *Effective surface areas of the CO_2 stores in the models.*

Store model	Cavern cross section	Surface area [m^2]
Single cavern	Small	13125
Single cavern	Large	11126
Dual cavern	Small	13808
Dual cavern	Large	12284

The storage of cold liquid CO_2 in warm bedrock causes an expanding temperature disturbance. As the storage temperature is well below the freezing point of water, it also creates an expanding frozen zone around the store. Appendices A1–A24 illustrate the temporal evolution of the temperature disturbance created by the store and the edge of the freezing front and their radii for each simulation. The temperature disturbance was calculated as the temperature difference

between ground temperatures simulated with and without the CO_2 store. The radii of the disturbance contours and the frozen zone were calculated as the average distances between the store midpoint and the points on the contours and on the edge of the freezing front respectively. Fig. 19 illustrates the magnitude of the temperature disturbance in the upper 20 metres of the ground after 100 years of storage.

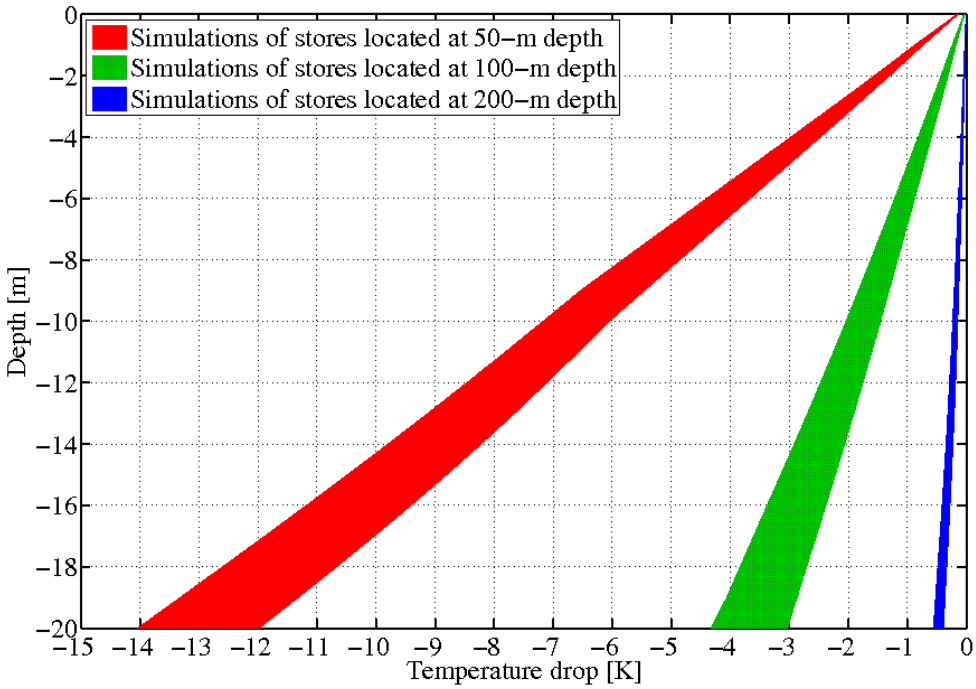

Figure 19. *Drop in upper ground temperatures after 100 years of CO_2 storage. Each coloured region in the plot shows the range that temperatures dropped in the simulations of stores at the specified depths due to CO_2 storage relative to undisturbed ground temperatures.*

4 Conclusions

Storing liquid CO_2 at the temperature of −40 °C directly to warm bedrock induces a large heat flow into the store during the first year of storage as is evident from Fig. 18. As the stored liquid CO_2 needs to be kept constantly at a temperature close to −40 °C, this would require the installation of a cooling capacity of 1.2–1.5 MW depending on the chosen store geometry and depth. A more viable option is to cool the bedrock in the vicinity of the store with a cooling power of few hundreds of kilowatts for the first year or two. For example, according to the results presented in Fig. 18, the cooling capacity of 300 kW would be sufficient if the bedrock in vicinity of the store is first cooled for the first 9–20 months (depending on store geometry and depth) before the actual CO_2 storage.

The results presented in Fig. 18 indicate that the most efficient CO_2 store option is the single or dual cavern store with the large cavern cross section. In these cases, the total cavern wall surface area is minimized which also minimizes the heat flow into the store and the required cooling power to keep the stored CO_2 at a temperature close to −40 °C. Extrapolating from these results, the most optimal store geometry would be a spherical cavity while the least optimal geometry would be a long and narrow tunnel.

The results indicate that the optimal depth for the store is likely somewhere between 50 and 200 m as the stores located at 100-m depth appear to require the least amount of cooling power in the long run. However, there is no drastic difference between the required cooling powers between the stores located at any depth. Nevertheless, the stores located at 50 m depth appear to require somewhat more cooling power than the stores located deeper. This is because in the case of a shallow store, the temperature gradient between the ground surface and the store is steepest and the shallow store is more affected by solar heating than the deeper stores. Siting the store deeper than 200 m would likely increase the required cooling power because ground temperatures increase with depth.

The temperature disturbance created by the store expands rapidly during the first decades of storage. However, it remains low at the ground surface even after 100 years of storage, but becomes considerable when going downwards as is illustrated by Fig. 19. The temperature disturbance might have an influence on constructs either located or extending below the ground surface especially in the case of a shallow store.

5 References

Ahn, J., Headly, M., Wahlen, M., Brook, E.J., Mayewski, P. A., and Taylor, K.C., 2008. CO_2 diffusion in polar ice: observations from naturally formed CO2 spikes in the Siple Dome (Antarctica) ice core. Journal of Glaciology 54, 685–695.

Bateman, K., Rochelle, C.A., Purser, G., Kemp, S.J., and Wagner, D., 2013. Geochemical interactions between CO_2 and minerals within the Utsira caprock: A 5-year experimental study. Energy Procedia, 37, 5307–5314.

Chadwick, A., Arts, R., Bernstone, C., May, F., Thibeau, S., and Zweigel, P.R., 2008. Best practice for the storage of CO_2 in saline aquifers – observations and guidelines from the SACS and CO2STORE projects. British Geological Survey Occasional Publication 14, 267 p.

Deardorff, J.W., 1978. Efficient Prediction of Ground Surface Temperature and Moisture with Inclusion of a Layer of Vegetation. Journal of Geophysical Research 83, 1889–1903.

Fujii, H., Nishi, K., Komaniwa, Y., and Chou, N., 2012. Numerical modelling of slinky-coil horizontal ground heat exchangers. Geothermics 41, 55–62.

Gilgen, H., and Ohmura, A., 1999. The Global Energy Balance Archive (GEBA). Bulletin of the American Meteorological Society 80, 831–850.

Johansson, S., 1985. Engineering geological experience from Finland from unlined excavated oil storage caverns in a Precambrian rock mass in the Porvoo area, Southern Finland. Doctoral dissertation, University of Turku. Neste Oy, Finland. 77 p.

Koistinen, T. J. (ed.), 1996. Explanation to the map of Precambrian basement of the Gulf of Finland and surrounding area 1:1 million. Geological Survey of Finland, Special Paper 21, 141 p.

Kujanpää, L., Ritola, J., Nordbäck, N., and Teir, S., 2014. Scenarios and new technologies for a North-European CO_2 transport infrastructure in 2050. Energy Procedia 63, 2738–2756.

Kukkonen, I., 1989. Terrestrial heat flow in Finland, the central Fennoscandian Shield. Geological Survey of Finland, Report YST-68, 32 p.

Kukkonen, I., Kivekäs, L., Vuoriainen, S., and Kääriä, M., 2011. Thermal Properties of Rocks in Olkiluoto: Results of Laboratory Measurements 1994–2010. Posiva Oy, Working Report 2011-17, 96 p.

Peltoniemi, S., and Kukkonen, I., 1997. Thermal properties of rocks in Finland. Vuorimiesyhdistys, Sarja A, 100 p.

Ritola, J., Kujanpää, L., Lindberg, A., and Nordkbäck, N., 2014. CLEEN–CCS Task 4.21. CO_2 Terminals and Intermediate storage. CLEEN Ltd., Final Report 2013, 42 p.

Seemann, S.W., Borbas, E.E., Knuteson, R.O., Stephenson, G.R., Huang, H.-L., 2007. Development of a Global Infrared Land Surface Emissivity Database for Application to Clear Sky

Sounding Retrievals from Multi-spectral Satellite Radiance Measurements. Journal of Applied Meteorology and Climatology 47, 108–123.

SLR, 2014. Final Report on Prospective Sites for the Geological Storage of CO_2 in the Southern Baltic Sea. URL: https://www.energimyndigheten.se/Global/Forskning/Br%C3%A4nsle/CCS%20-%20BASTOR2/140324%20%20BASTOR%20Final%20Report.pdf

Teir, S., Arasto, A., Tsupari, E., Koljonen, T., Kärki, J., Kujanpää, L., Lehtilä, A., Nieminen, M., and Aatos, S., 2011. Hiilidioksidin talteenoton ja varastoinnin (CCS:n) soveltaminen Suomen olosuhteissa – Application of carbon capture and storage (CCS) in Finnish conditions. VTT Technical Research Centre of Finland Ltd., VTT Research Notes 2576, 76 p.

Vangkilde-Pedersen, T., Kirk, K., Smith, N., Maurand, N., Wojcicki, A., Neele, F., Hendriks, C., Le Nindre, Y.-M., Anthonsen, K.L., 2009. EU Geocapacity – Assessing European Capacity for Geological Storage of Carbon Dioxide. D42 GeoCapacity Final Report. URL: http://www.geology.cz/geocapacity/publications

6 Appendices

A1Single cavern, small cross section, no cooling, located at 50 m depth

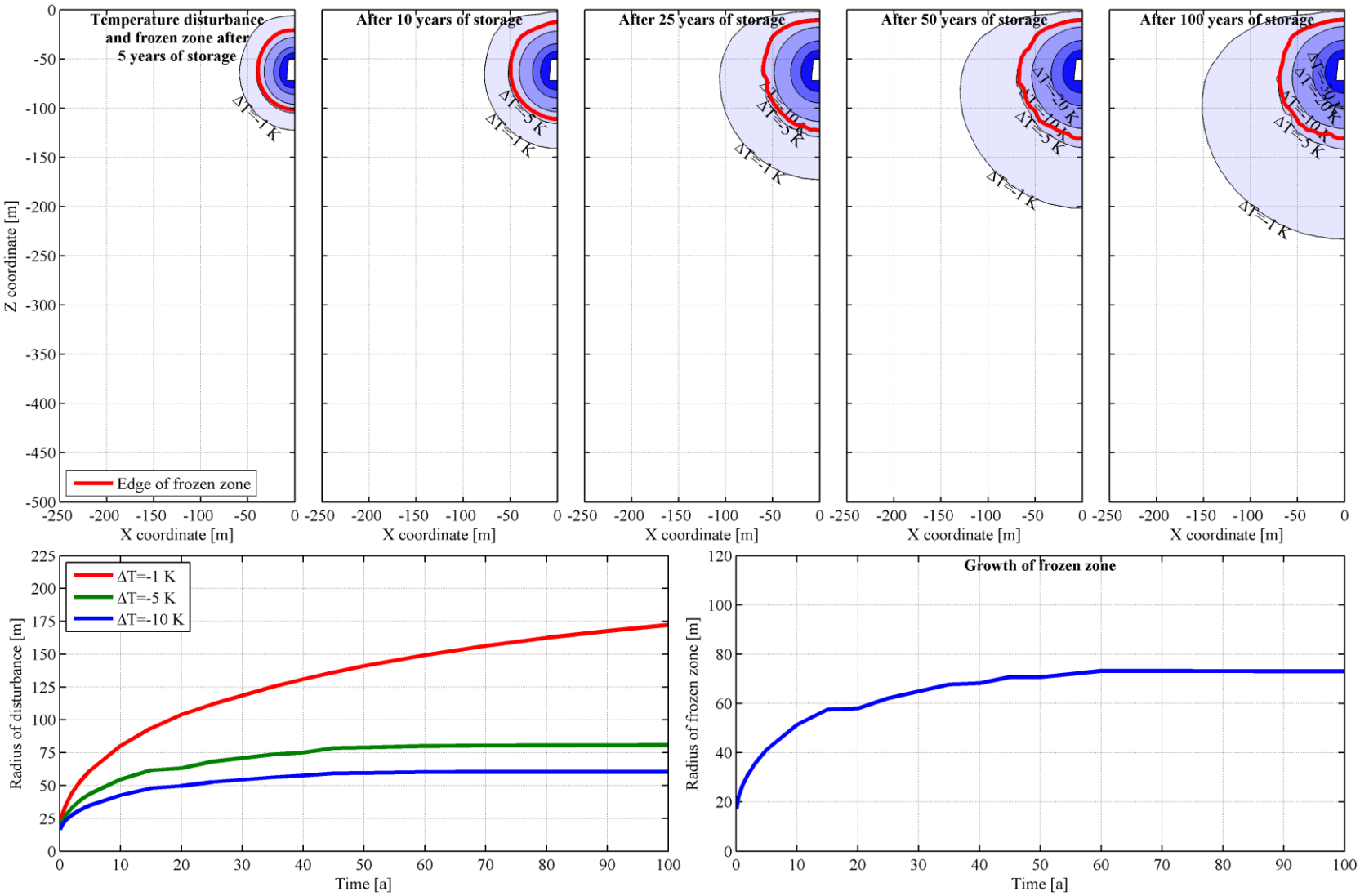

A2Single cavern, small cross section, no cooling, located at 100 m depth

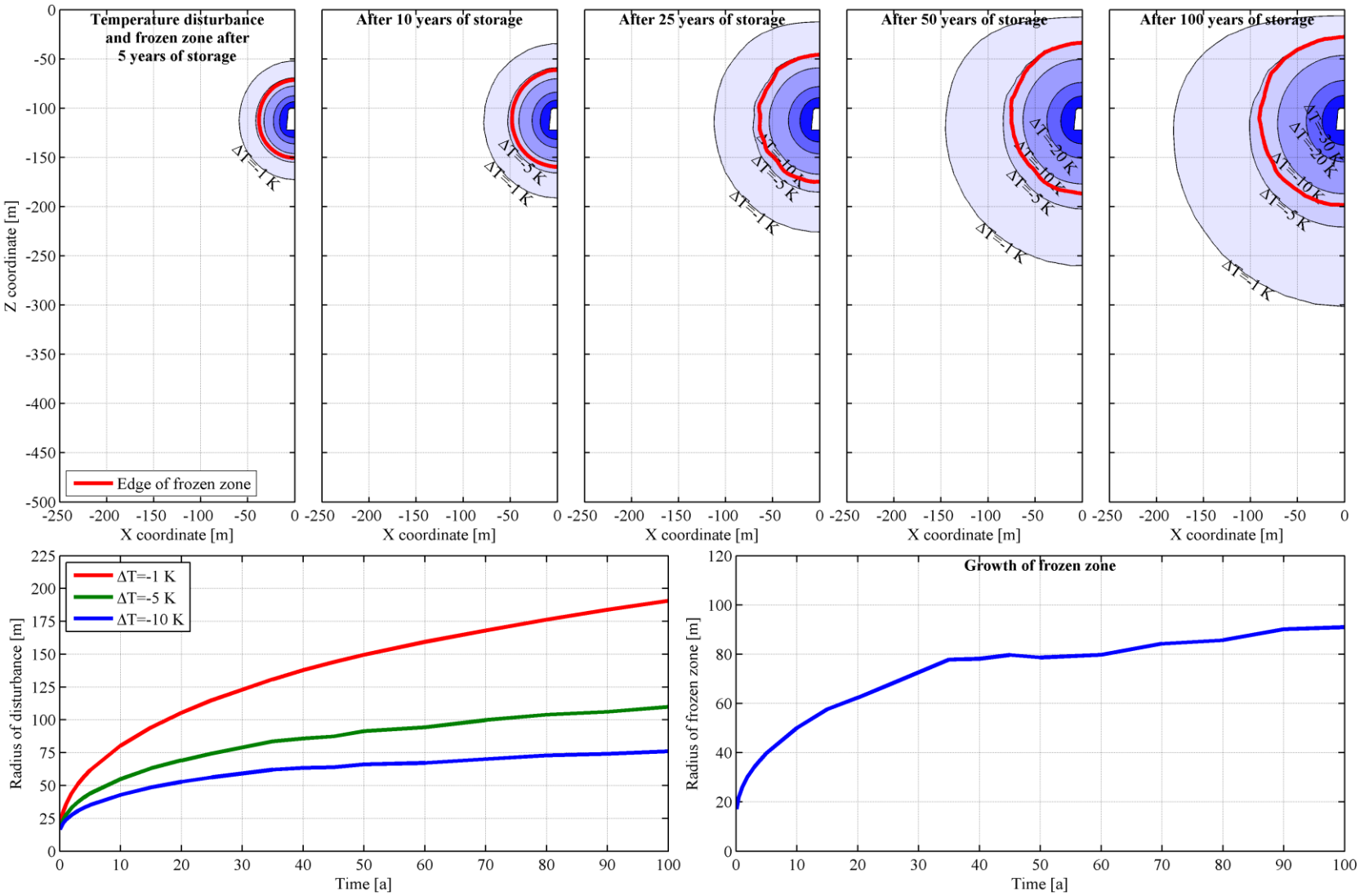

A3Single cavern, small cross section, no cooling, located at 200 m depth

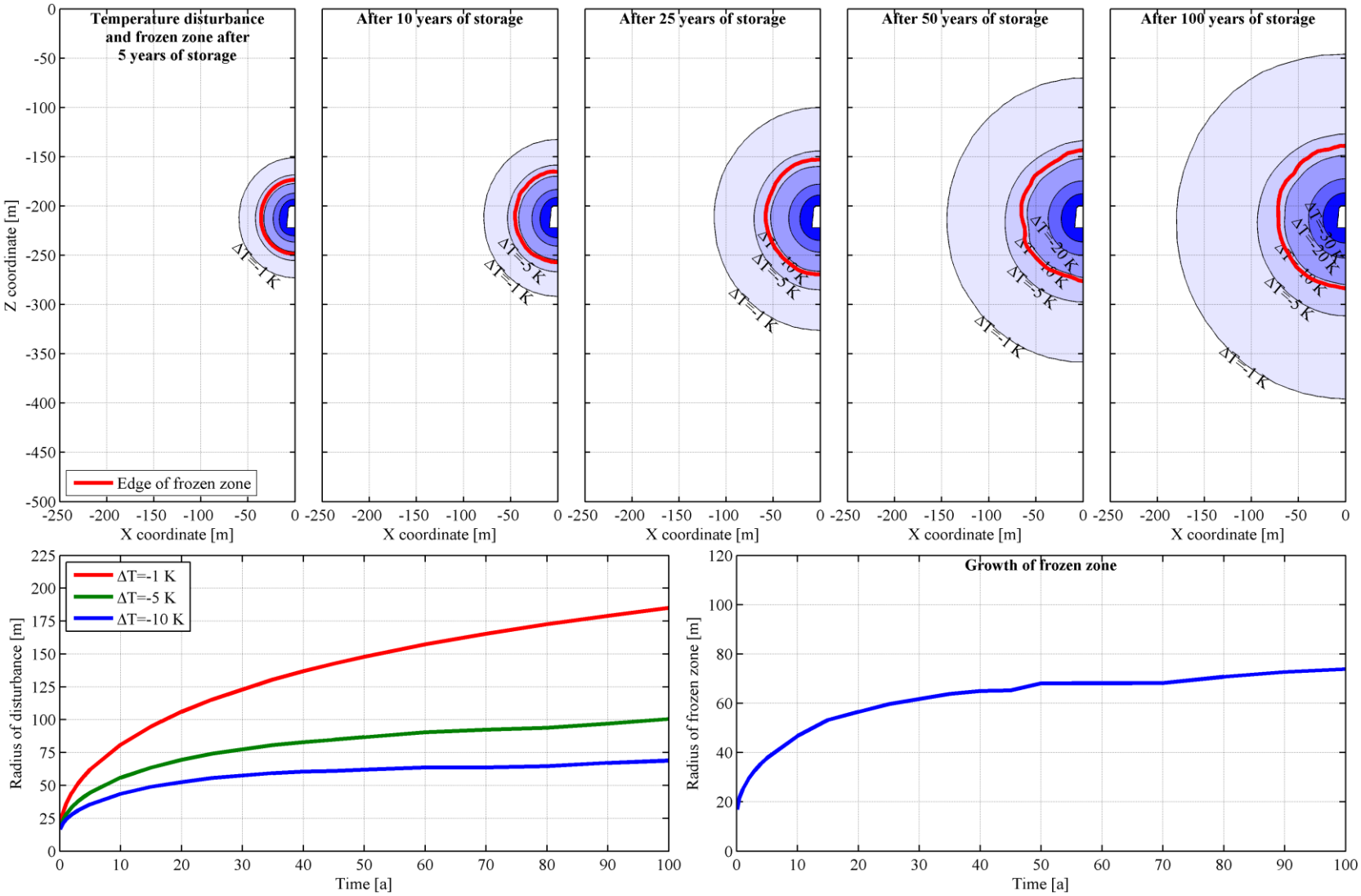

A4Single cavern, small cross section, with cooling, located at 50 m depth

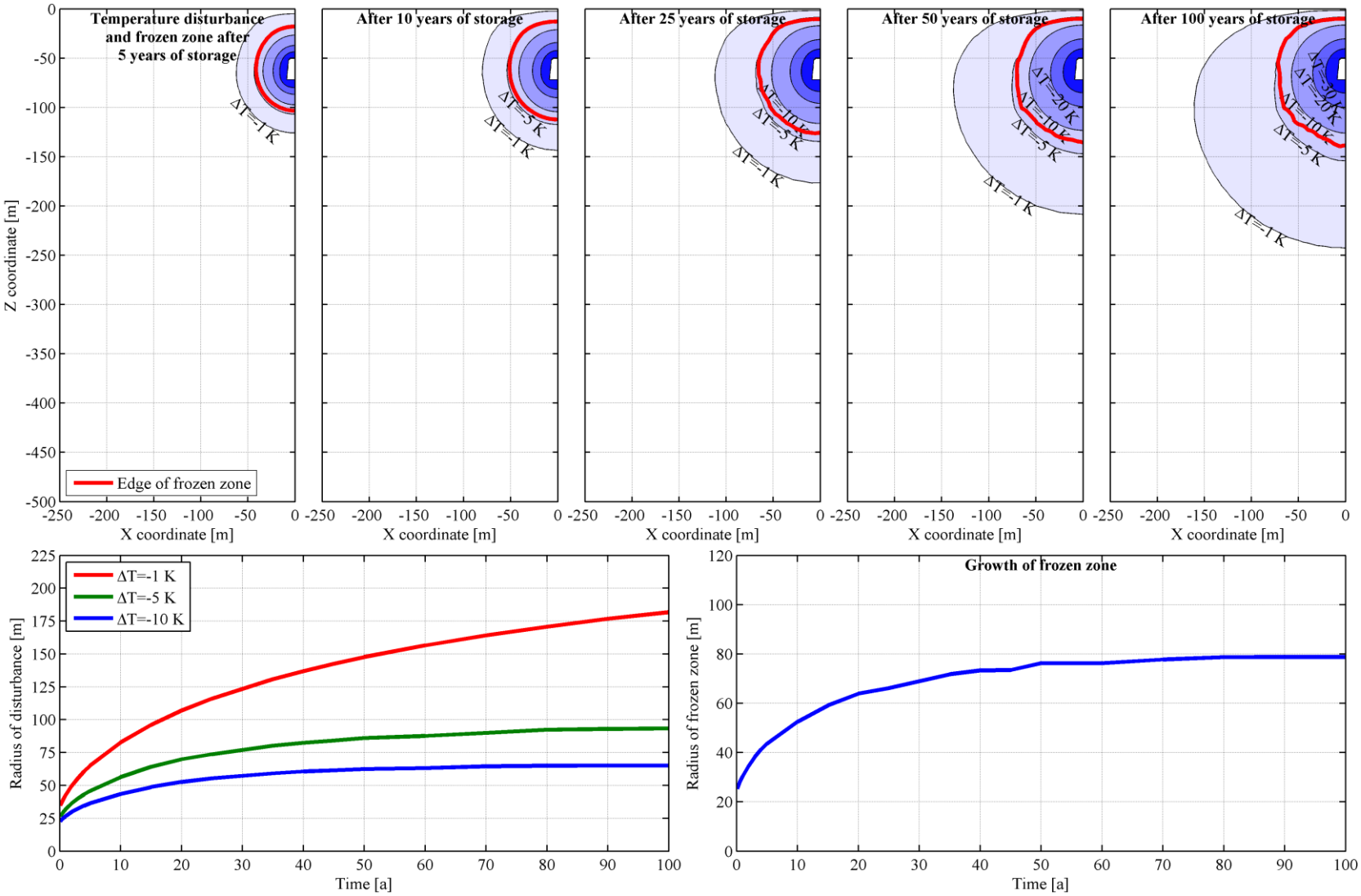

A5Single cavern, small cross section, with cooling, located at 100 m depth

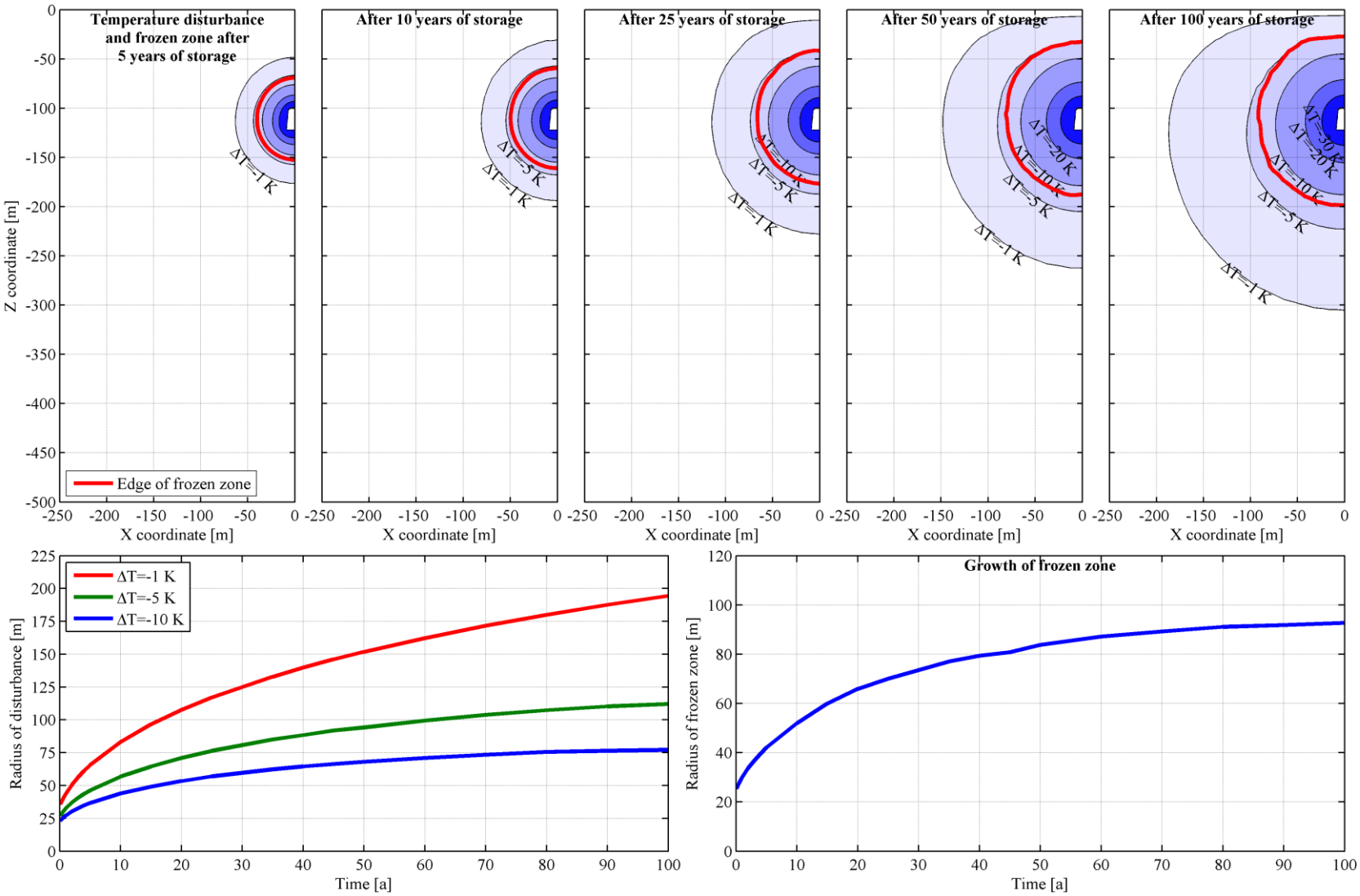

A6Single cavern, small cross section, with cooling, located at 200 m depth

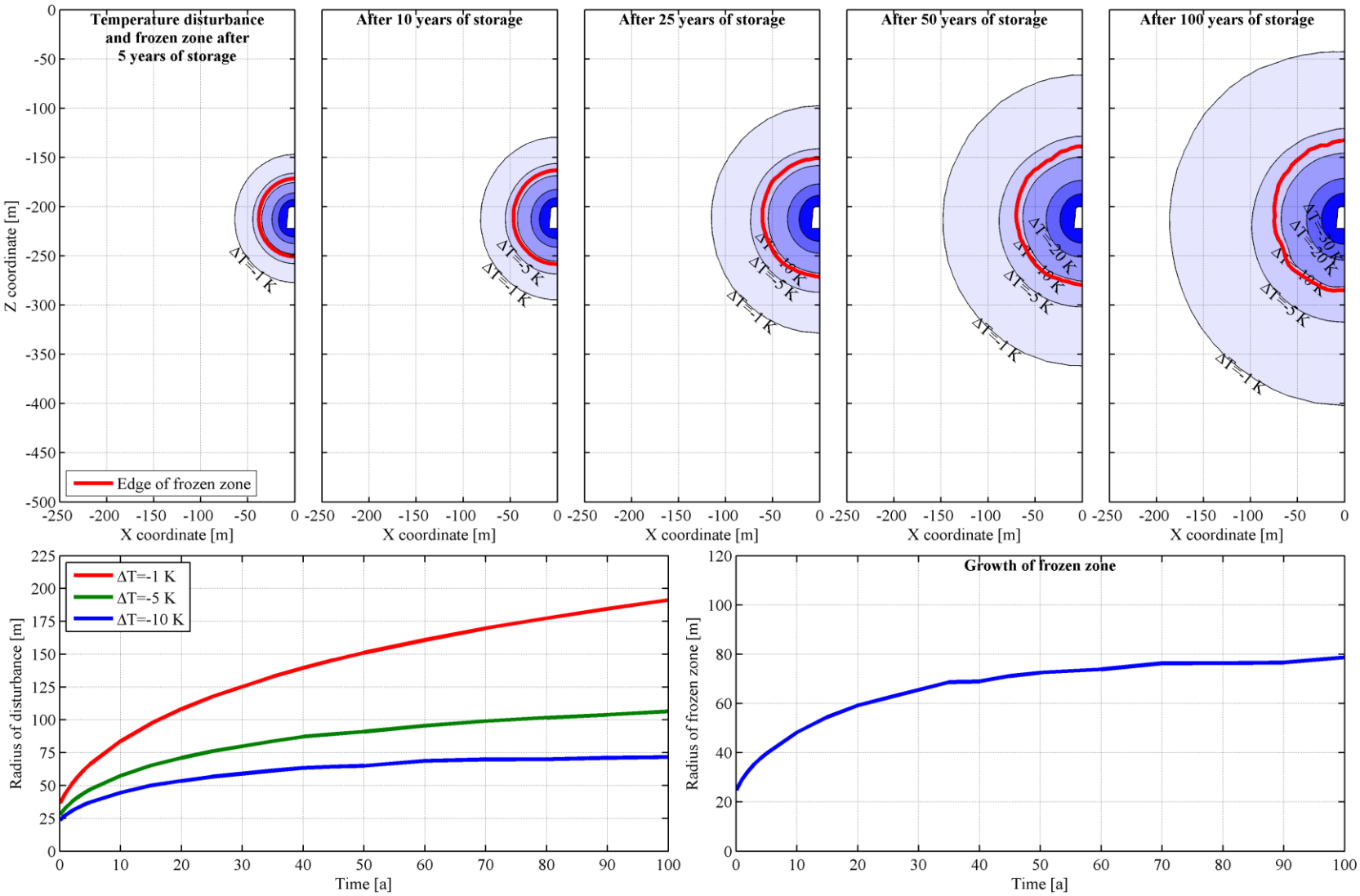

A7Single cavern, large cross section, no cooling, located at 50 m depth

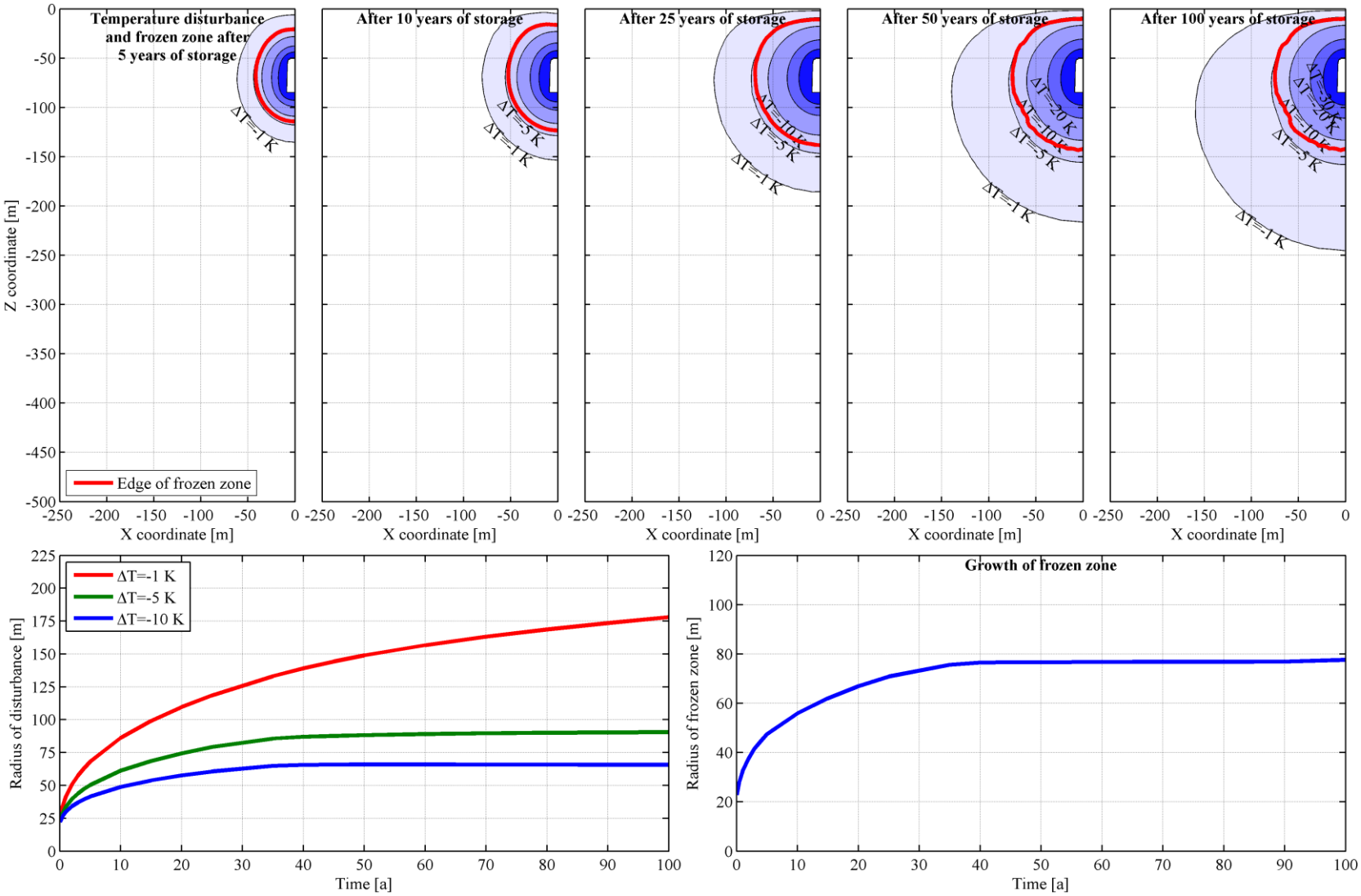

A8Single cavern, large cross section, no cooling, located at 100 m depth

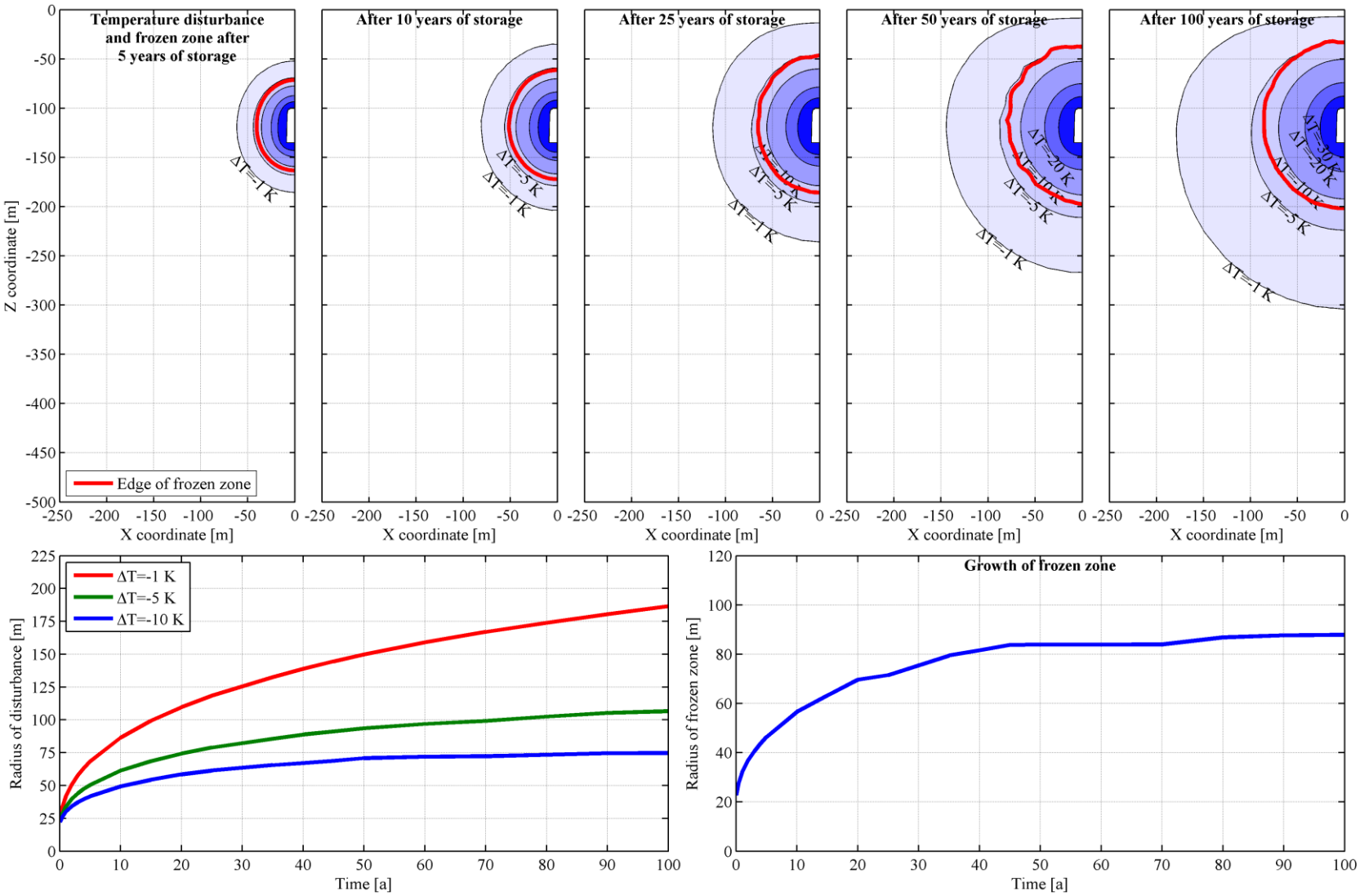

A9Single cavern, large cross section, no cooling, located at 200 m depth

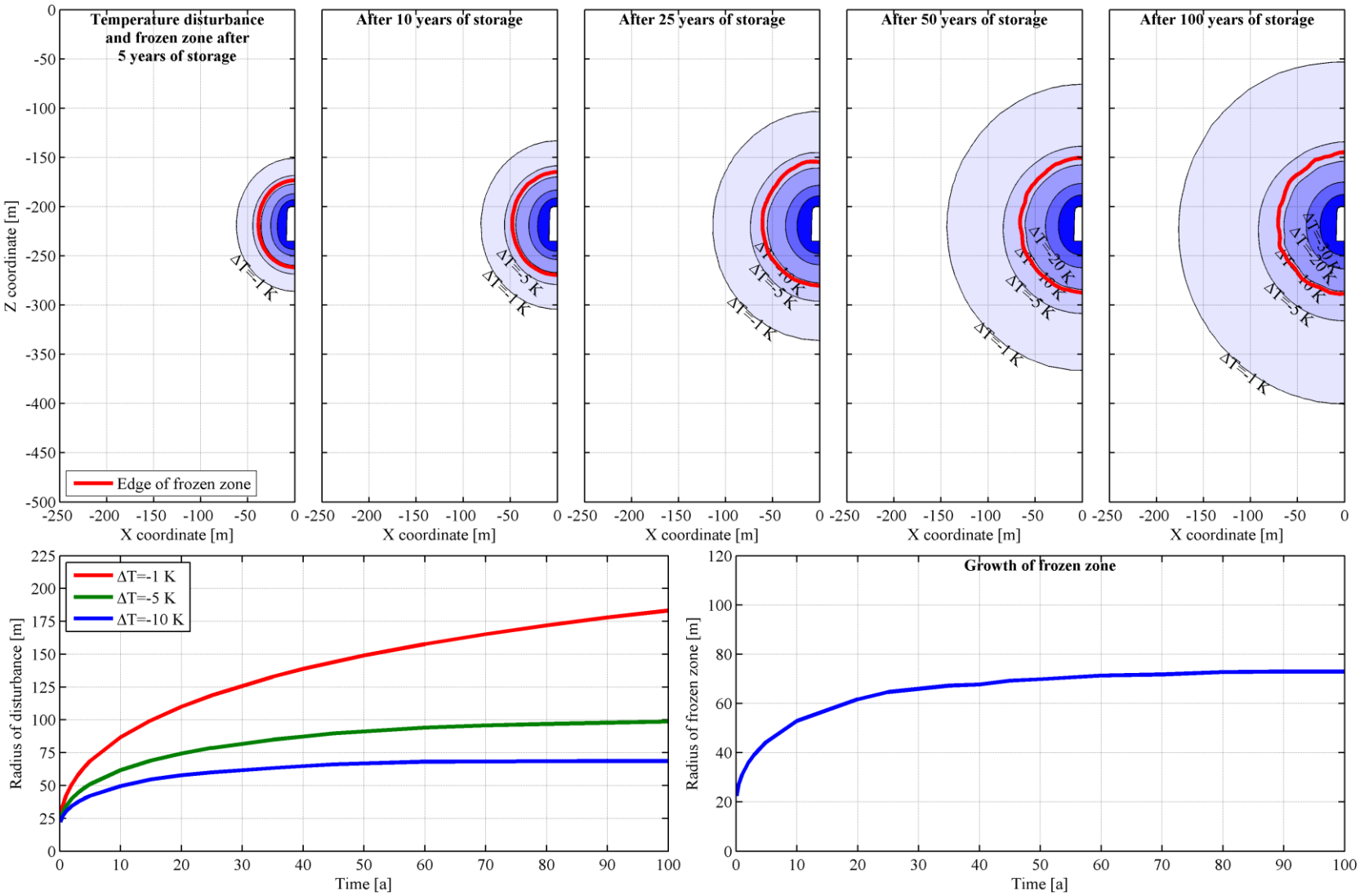

A10 Single cavern, large cross section, with cooling, located at 50 m depth

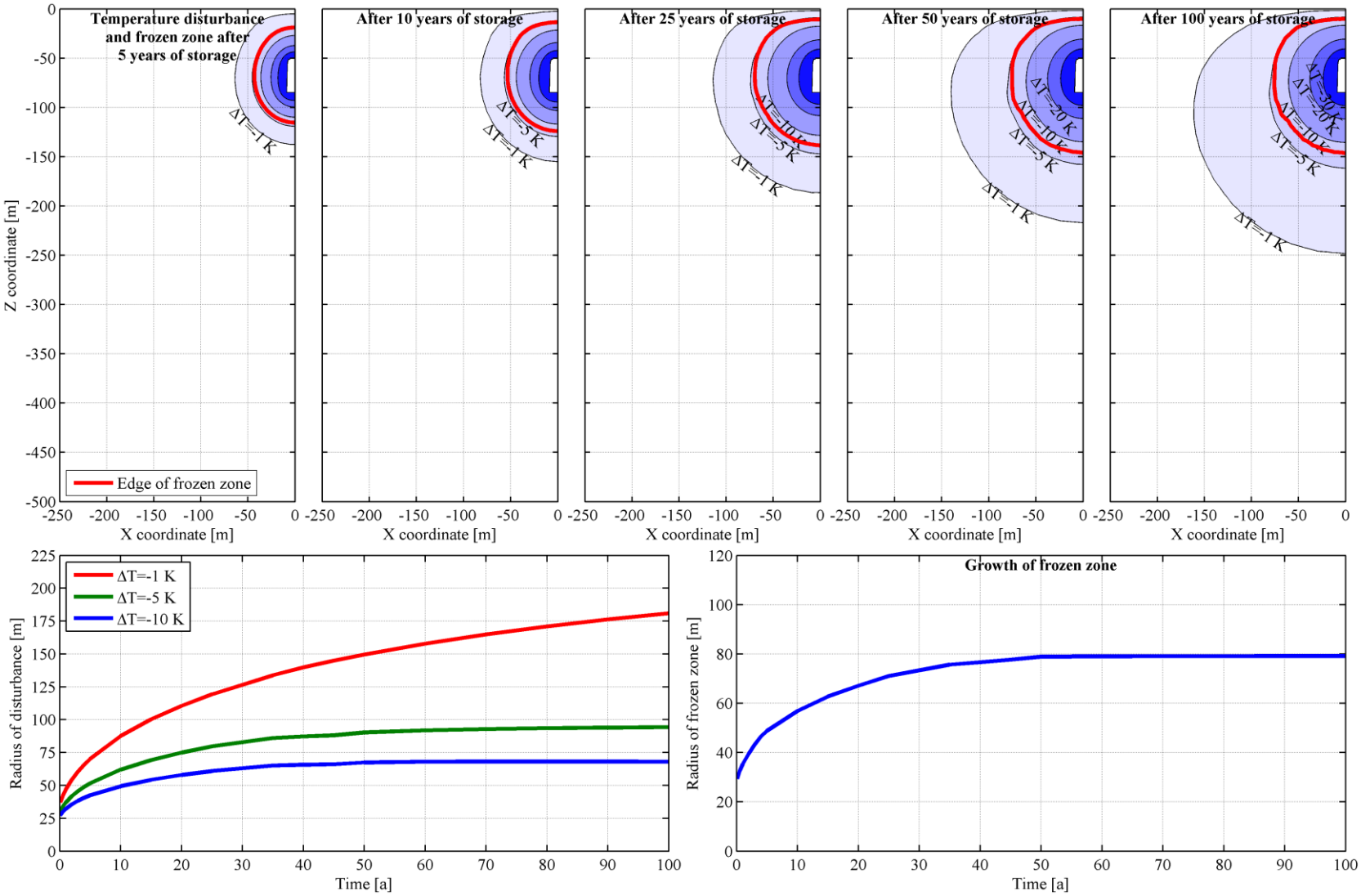

A11 Single cavern, large cross section, with cooling, located at 100 m depth

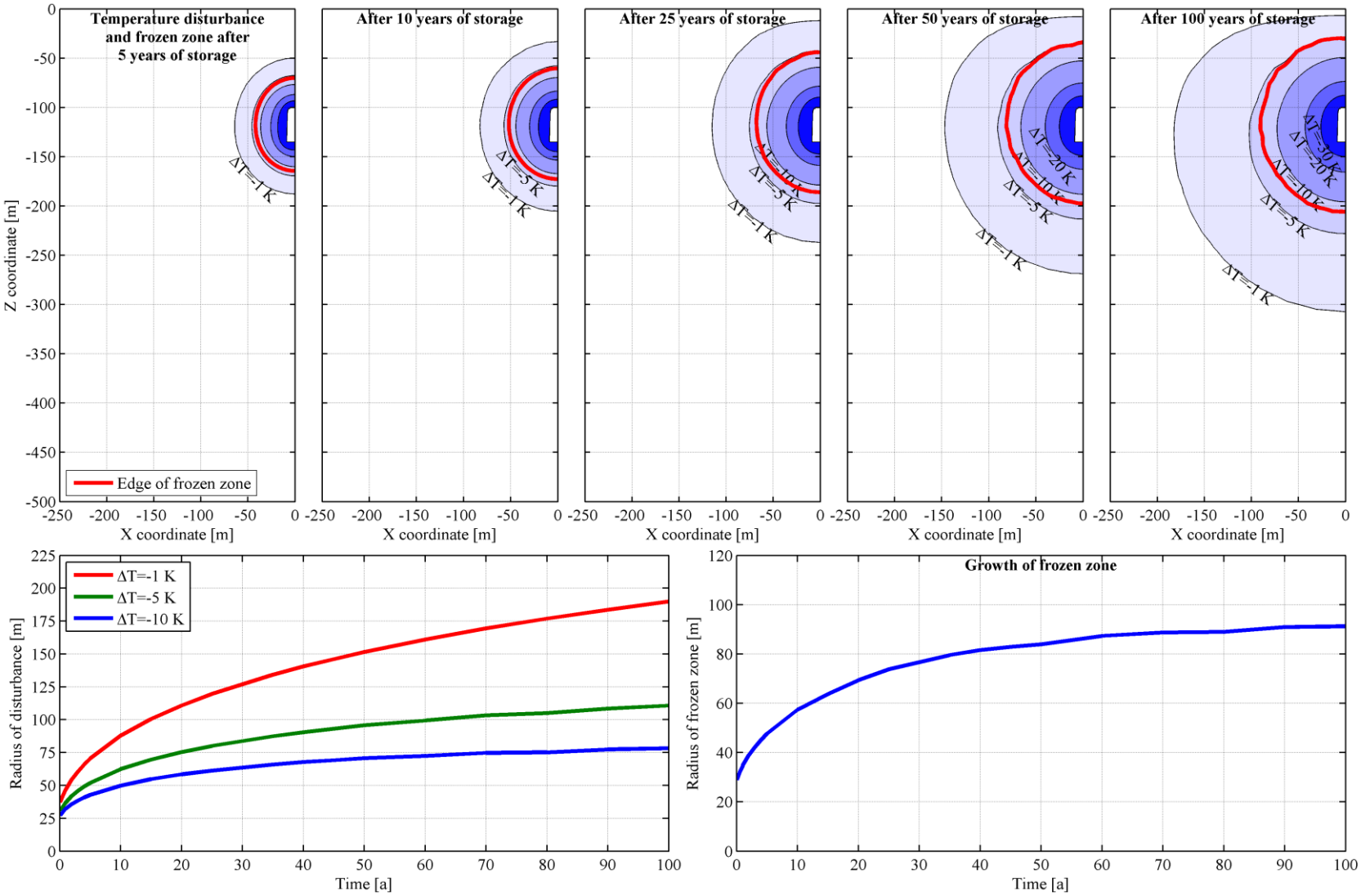

A12 Single cavern, large cross section, with cooling, located at 200 m depth

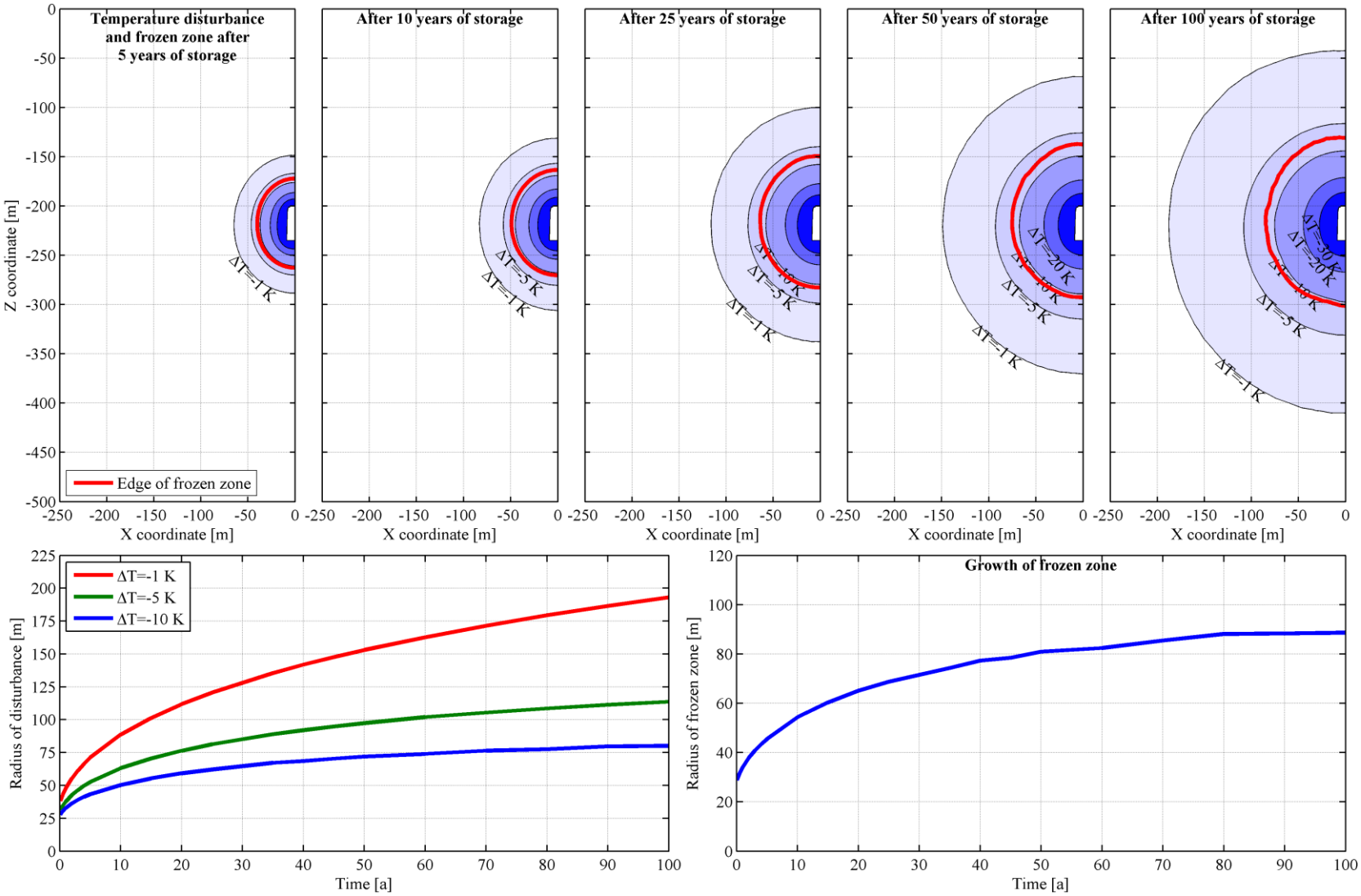

A13 Dual cavern, small cross section, no cooling, located at 50 m depth

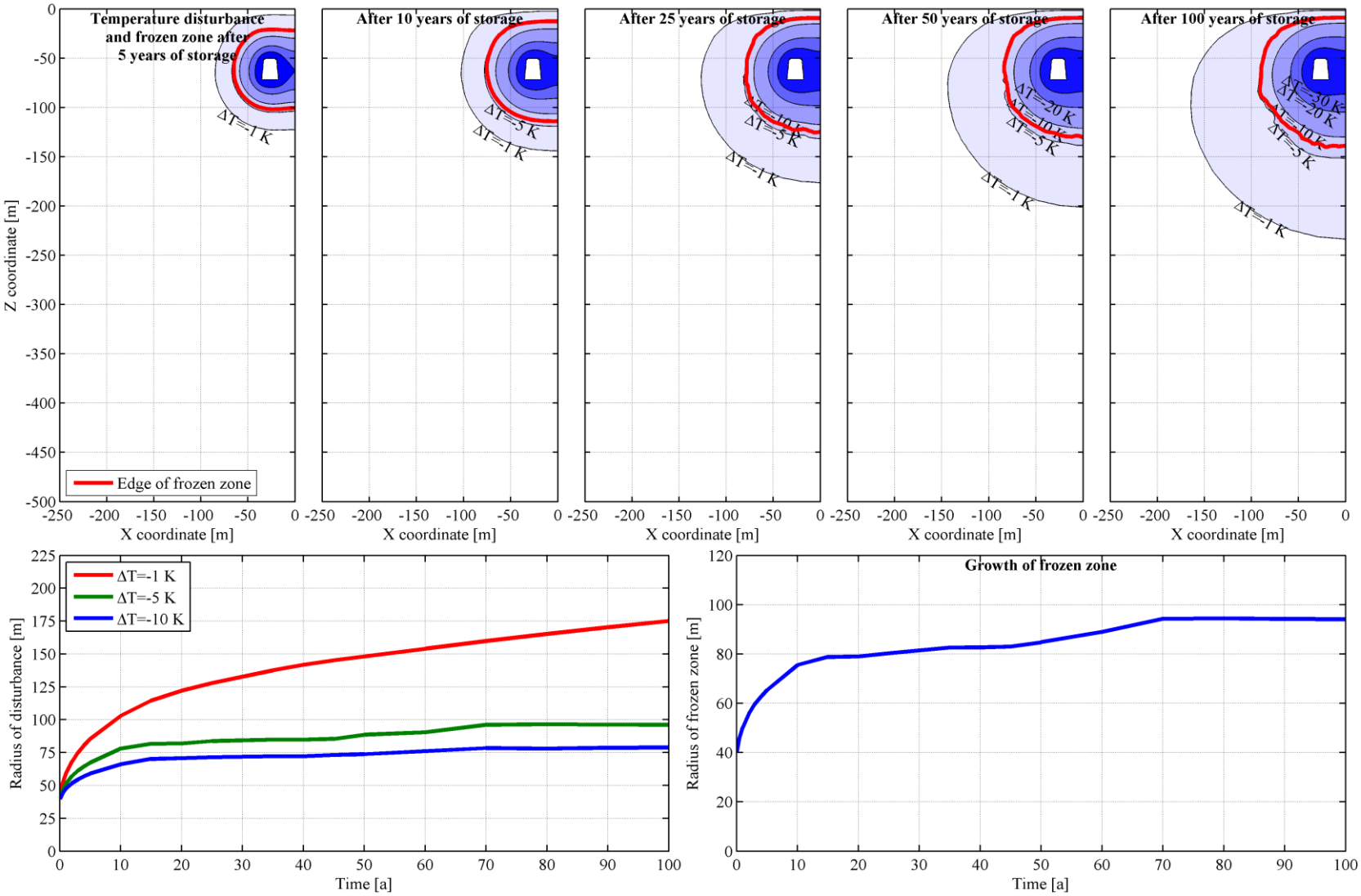

A14 Dual cavern, small cross section, no cooling, located at 100 m depth

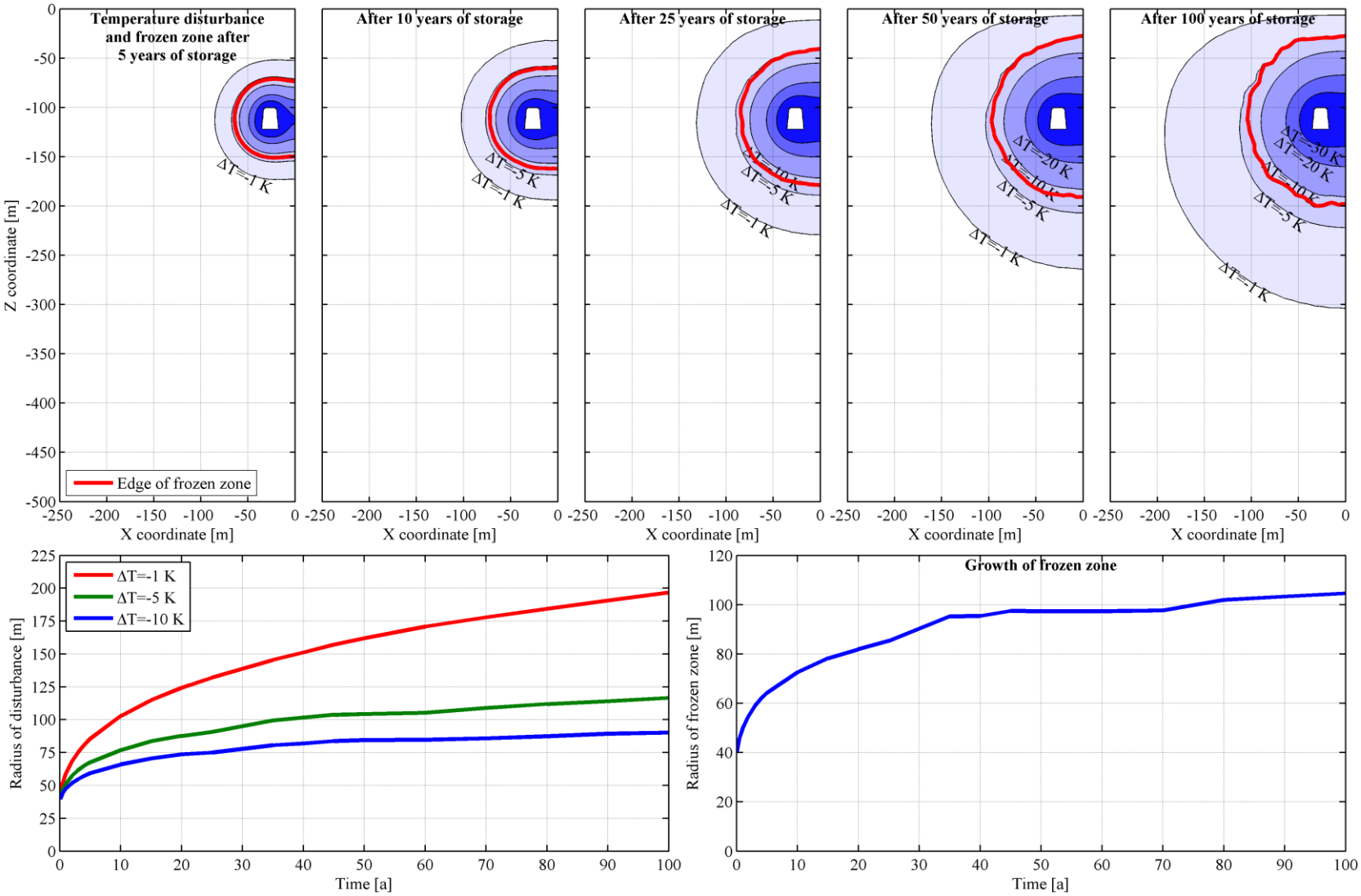

A15 Dual cavern, small cross section, no cooling, located at 200 m depth

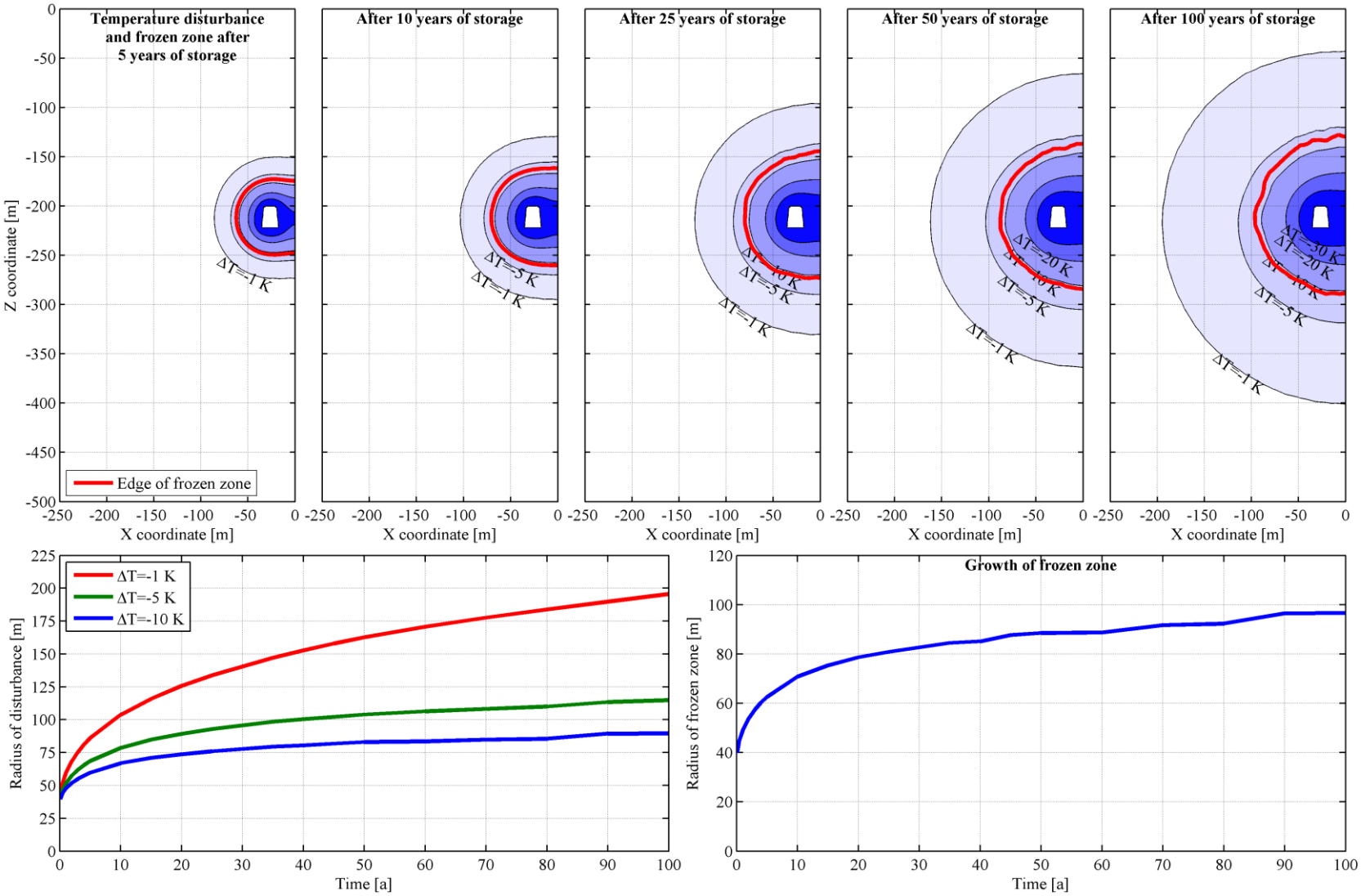

A16 Dual cavern, small cross section, with cooling, located at 50 m depth

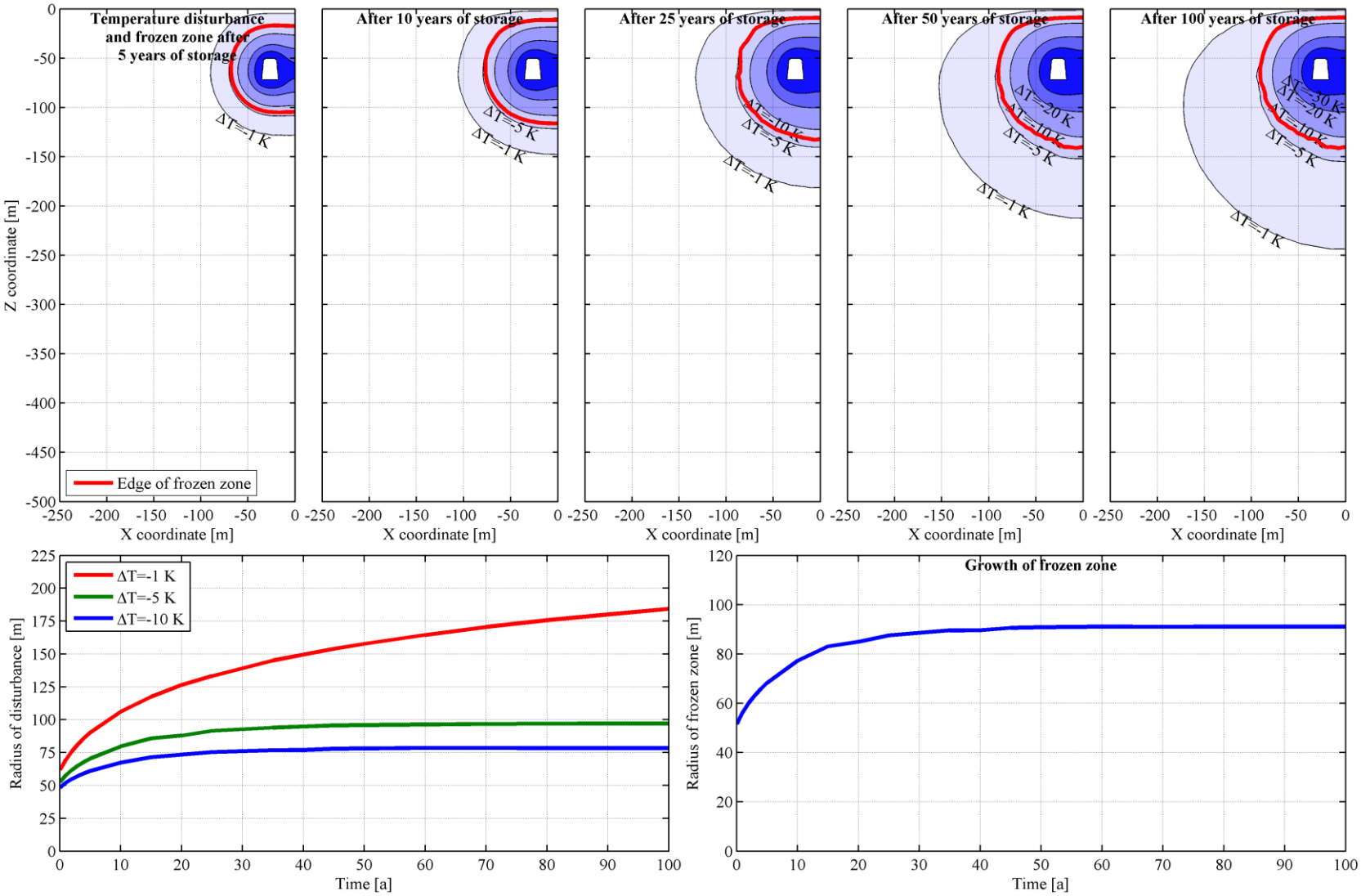

A17 Dual cavern, small cross section, with cooling, located at 100 m depth

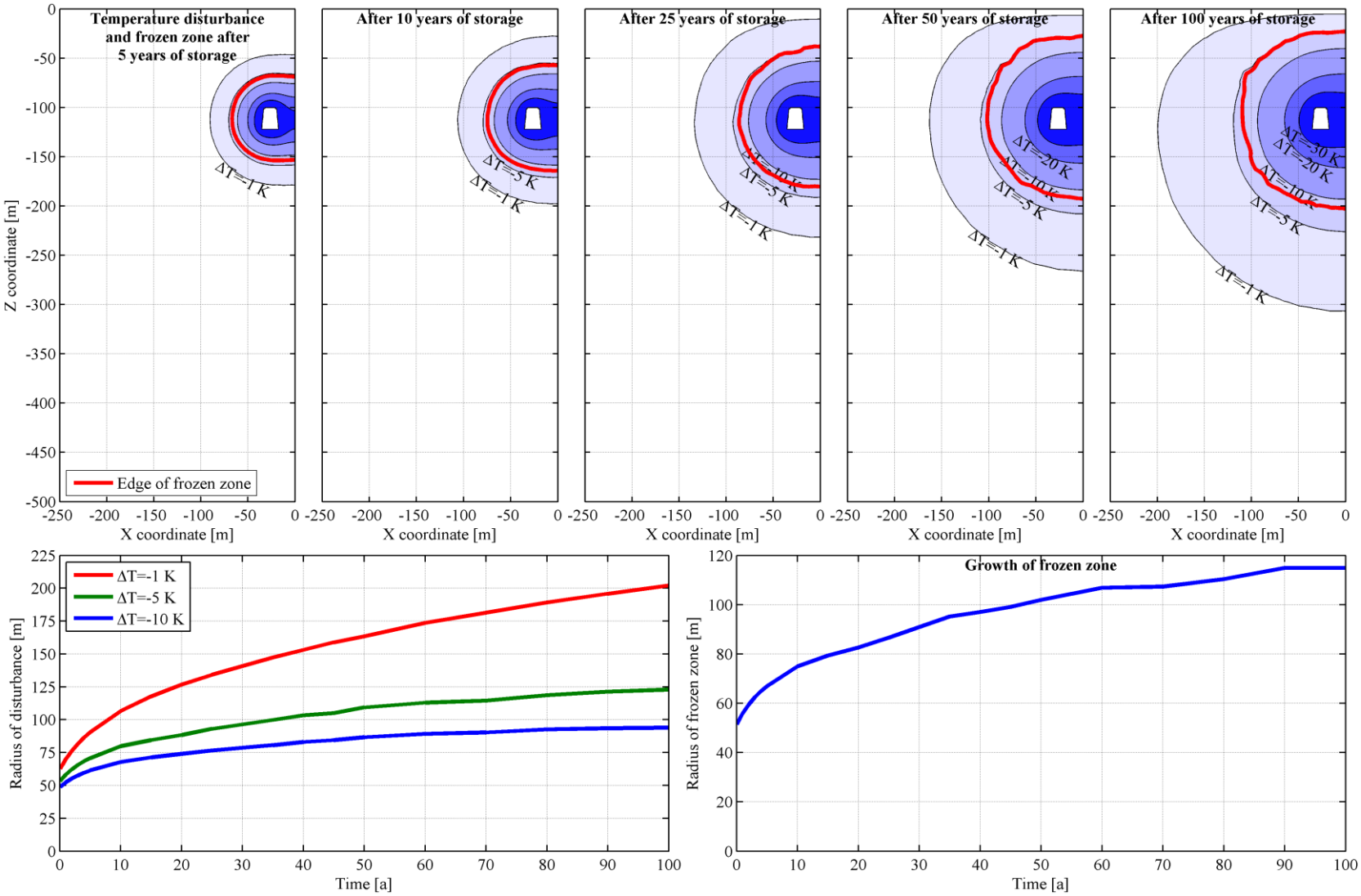

A18 Dual cavern, small cross section, with cooling, located at 200 m depth

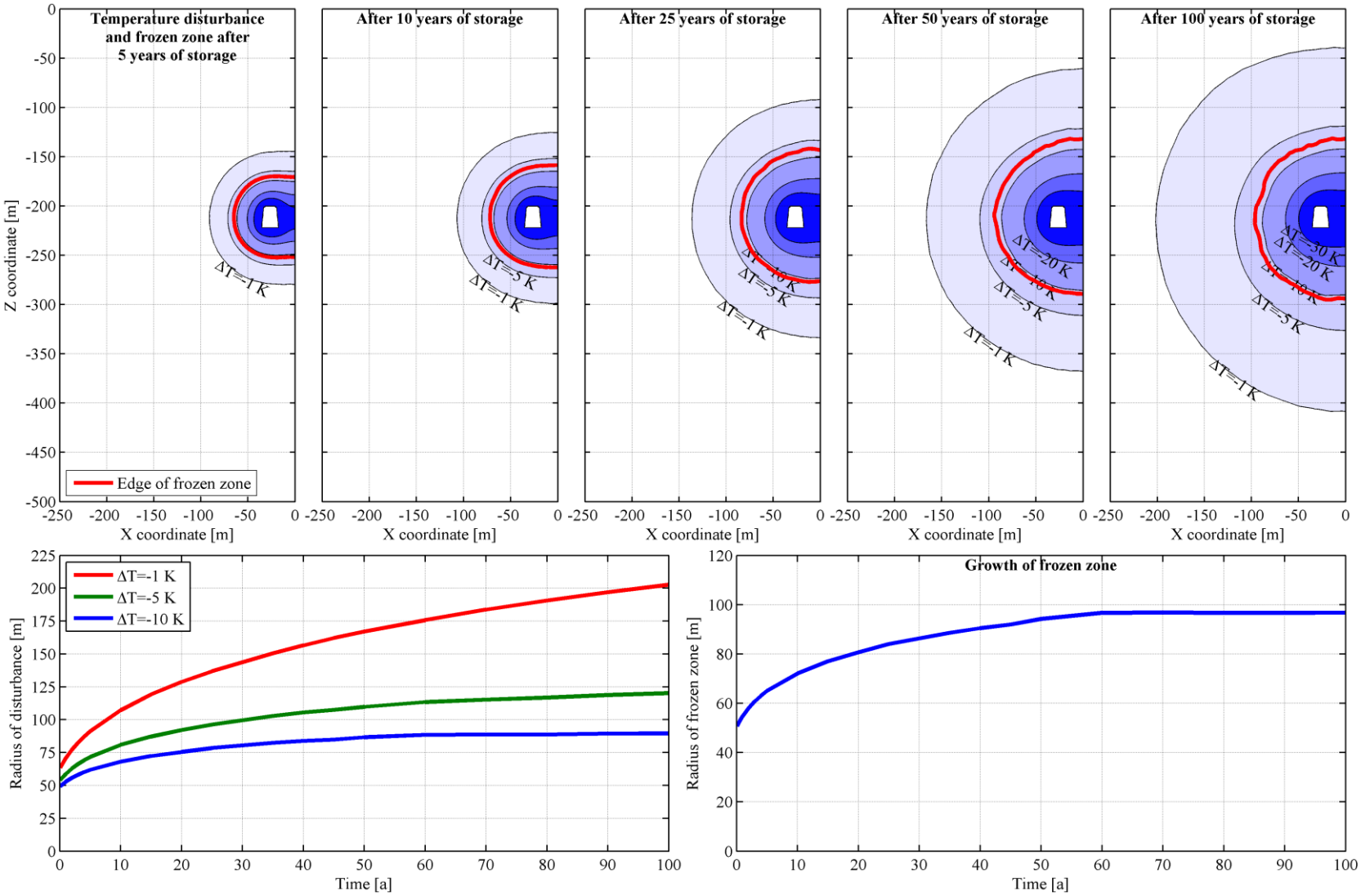

A19 Dual cavern, large cross section, no cooling, located at 50 m depth

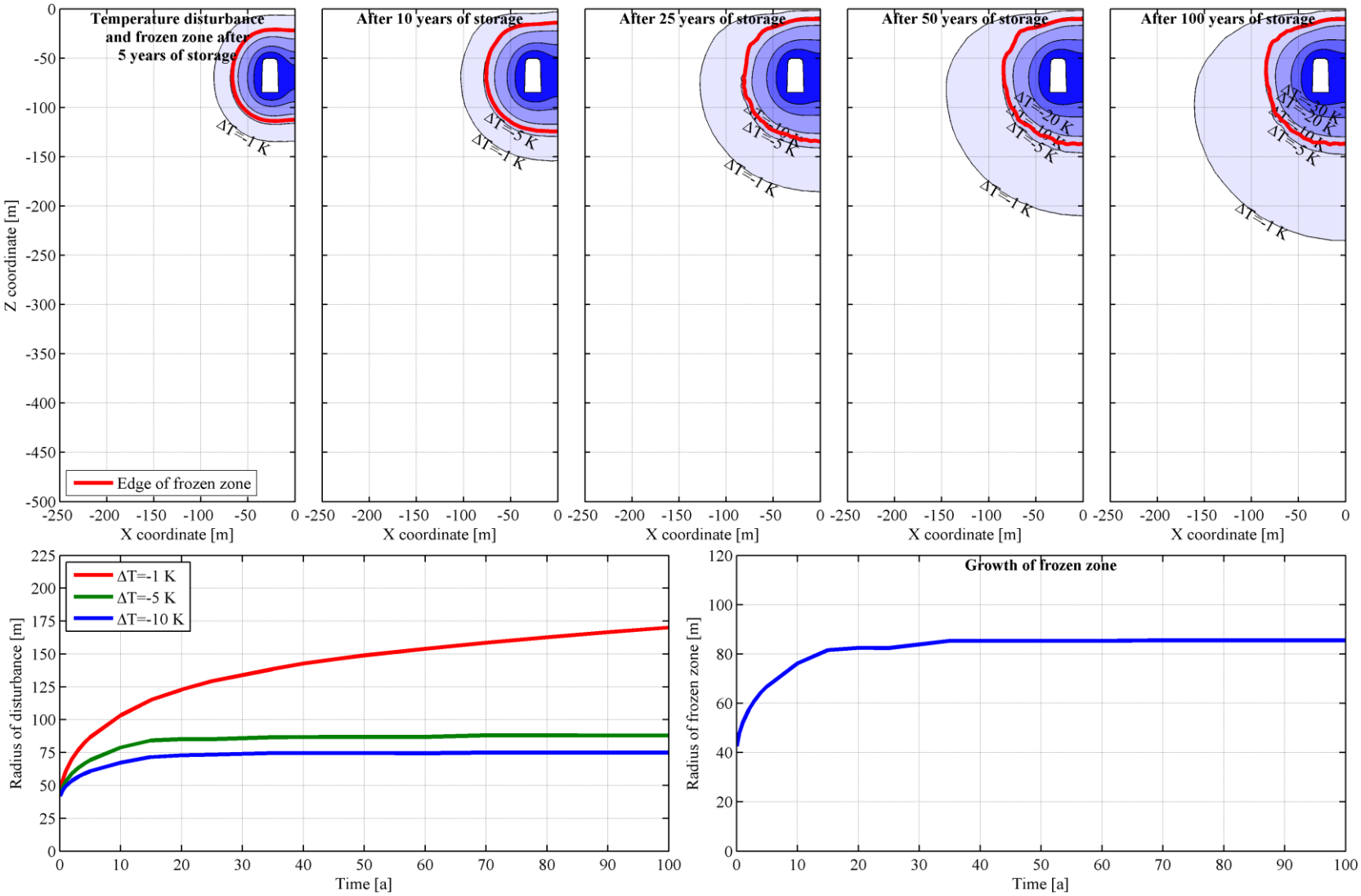

A20 Dual cavern, large cross section, no cooling, located at 100 m depth

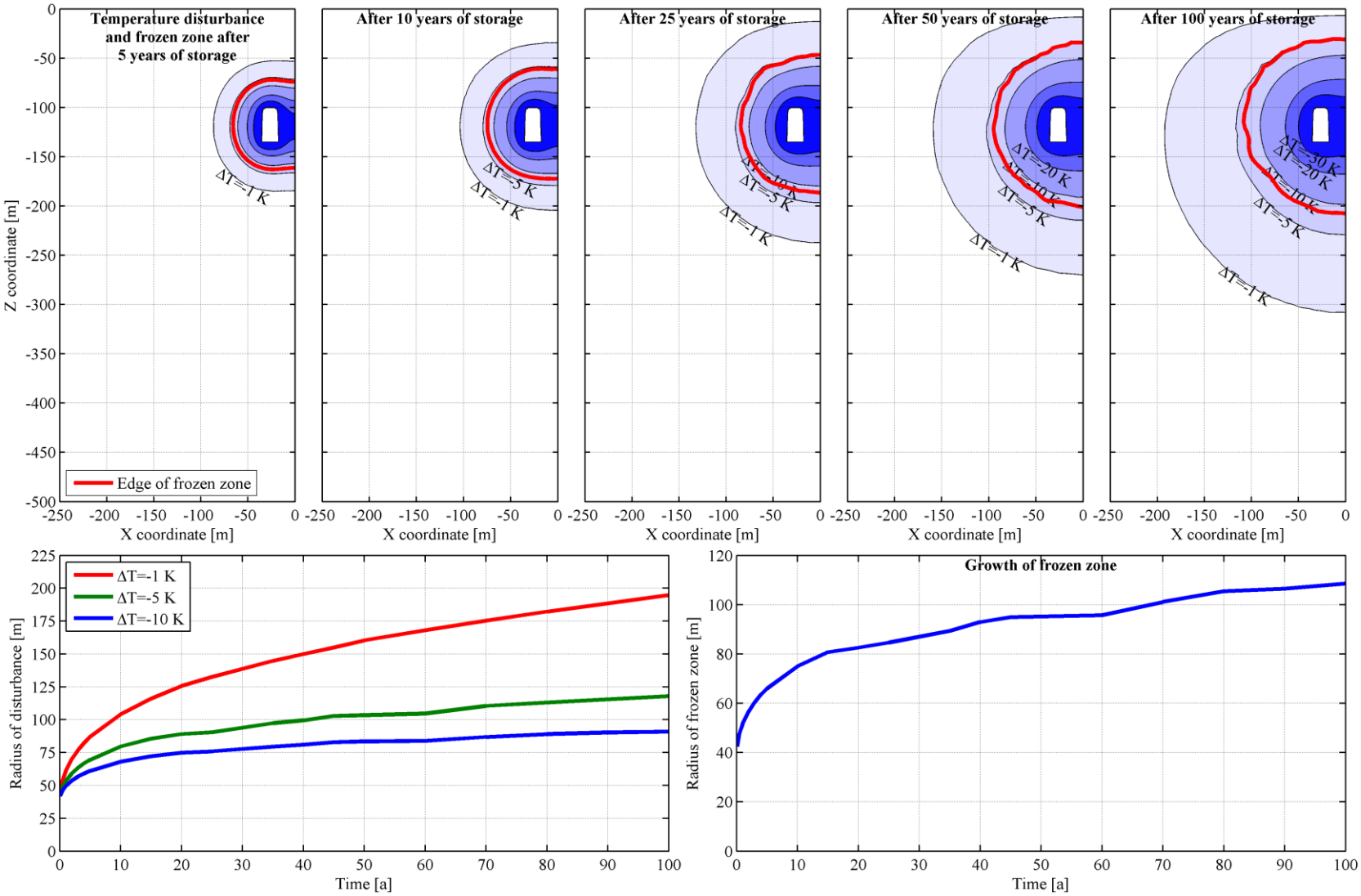

A21 Dual cavern, large cross section, no cooling, located at 200 m depth

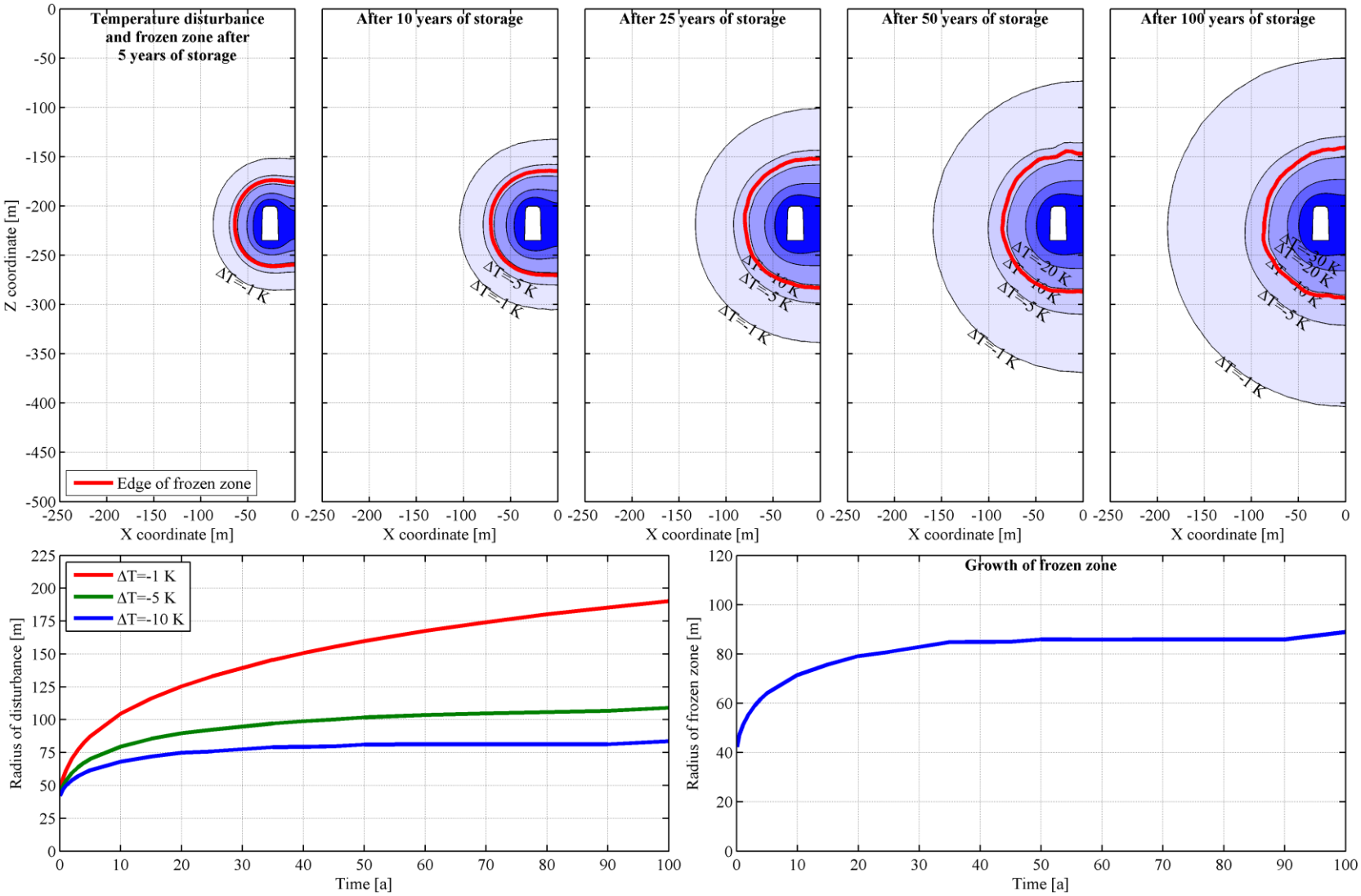

A22 Dual cavern, large cross section, with cooling, located at 50 m depth

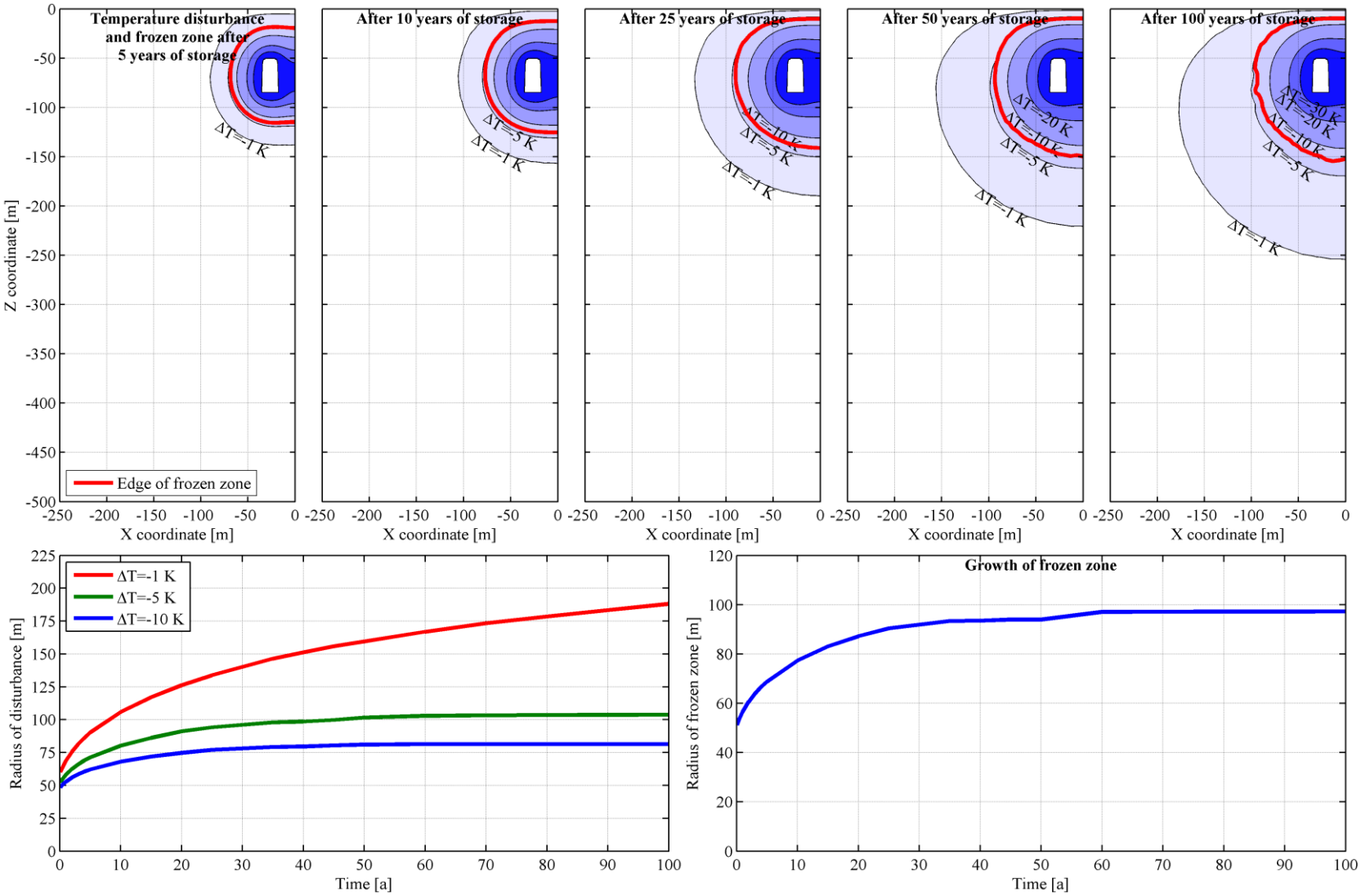

A23 Dual cavern, large cross section, with cooling, located at 100 m depth

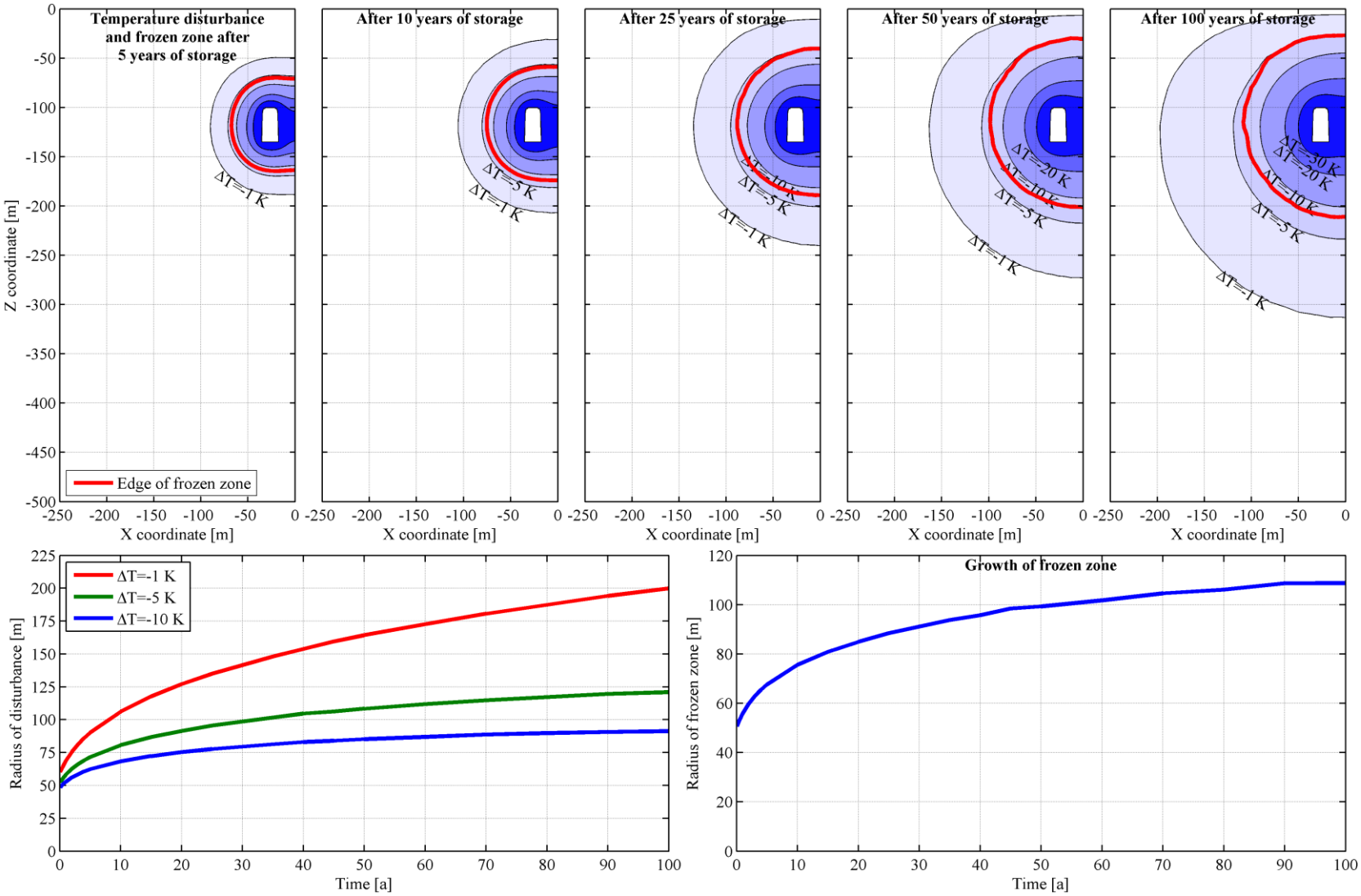

A24 Dual cavern, large cross section, with cooling, located at 200 m depth